Identifying regions that can constrain anthropogenic Hg emissions uncertainties through modelling

[1], Charikleia Gournia[1], Noelle E. Selin[2,3], and Aryeh Feinberg[4]

[1]Jožef Stefan International Postgraduate School, Ljubljana, Slovenia
[2]Department of Earth, Atmospheric and Planetary Sciences, Massachusetts Institute of Technology, Cambridge, MA, USA
[3]Institute for Data, Systems, and Society, Massachusetts Institute of Technology, Cambridge, MA, USA
[4]Department of Atmospheric Chemistry and Climate, Institute of Physical Chemistry Blas Cabrera, CSIC, Madrid, Spain

Correspondence: Charikleia Gournia (chgournia@gmail.com) and Noelle E. Selin (selin@mit.edu)

Abstract.

Anthropogenic mercury (Hg) emissions are a major contributor to global Hg pollution~~, however,~~ . However, limitations in emission inventories and modeling approaches impede accurate quantification of Hg emissions and Hg ~~inputs into ecosystems and complicate~~ ecosystem inputs, complicating the evaluation of ~~Hg~~ mitigation policies. This study investigates how ~~anthropogenic emissions uncertainty compared to other modeling uncertainties could~~ uncertainties in anthropogenic emissions, compared to chemistry and meteorology modeling uncertainties, affect model performance in model-observation comparisons, and explores strategies to evaluate ~~anthropogenic~~ emission uncertainties. We performed modeling experiments ~~that incorporated~~ using four global anthropogenic emission inventories~~(AMAP/GMA, EDGAR, STREETS, WHET), which have differences between them of~~ , which differ in Hg emissions by up to 630 ~~Mg for Hg emissions~~ Mg in Asia, 259 Mg in South America, and 252 Mg in Africa. We ~~also~~ employed two different chemical schemes and two meteorological datasets. ~~We found that the differences in anthropogenic Hg emission inventories~~ Inventory differences were the primary driver of ~~significant differences across the~~ differences across modeled total gaseous mercury ~~(TGM)~~ concentrations in the Northern Hemisphere, resulting in ~~a range~~ ranges of up to 0.47 ng m^{-3} in China and 0.32 ng m^{-3} in India~~in the mean of TGM concentrations in these regions~~. These differences ~~in modeling outputs can affect the~~ influenced Root Mean Square Error scores in ~~the TGM model-observation comparisonsthat can range~~ gaseous elemental mercury model–observation comparisons, ranging from 0.03 to ~~0.19~~ 0.17 in Asia, ~~from 0.12 to 0.25~~ 0.14 to 0.27 in the Arctic, and ~~from~~ 0.02 to 0.14 in the USA in an annual mean. ~~We conduct a~~ A signal-to-noise ratio (SNR) analysis ~~, identifying~~ identified regions such as the eastern U.S., Greenland, ~~and Arctic Russiathat could provide additional observational constraints on anthropogenic Hg emissions . In contrast, we show that the existing limited monitoring network in the Southern Hemisphere offers few~~ Arctic Russia, and parts of Asia and South America as valuable for constraining anthropogenic emissions at hemispheric scales. The existing Southern Hemisphere network offers limited constraints on emissions ~~,~~ but provides possible insights into Hg chemistry. These findings highlight the ~~critical~~ need for an expanded ~~global Hg~~ monitoring network and ~~more refined~~ improved emission inventories to reduce uncertainties and ~~improve the accuracy of~~ strengthen global Hg policy evaluation.

1 Introduction

Once mercury (Hg) is emitted into the atmosphere from human activities, it initiates a cycle of pollution in which Hg can circulate through the oceans, land, and air ~~Gustin et al. (2020)~~(Gustin et al., 2020). Estimating and projecting anthropogenic Hg emissions is of crucial importance for both scientific understanding and practical applications (e.g., policy-making) associated with harmful impact mitigation. There are several global ~~AMAP/UNEP (2019); Muntean et al. (2018); Streets et al. (2019); Zhang et al. (2~~(AMAP/UNEP, 2019; Muntean et al., 2018; Streets et al., 2019; Zhang et al., 2016), national and subnational ~~Zhang et al. (2015); Huang e~~(Zhang et al., 2015; Huang et al., 2017; Wu et al., 2016; Liu et al., 2019; Bich Thao et al., 2021; Zhang et al., 2023) anthropogenic Hg emissions inventories. Those constructing these inventories typically quantify and locate Hg-emitting activities, and then apply activity-specific emission factors to result in estimates of emissions in a bottom-up approach. Such inventories are comprehensive and have been used in studies with various scientific objectives ~~Shah et al. (2021); Mulvaney et al. (2020); Bruno et al. (2023); Fein~~(Shah et al., 2021; Mulvaney et al., 2020; Bruno et al., 2023; Feinberg et al., 2024a). However, significant uncertainty in emission inventories is introduced by estimates and assumptions ~~regarding~~ related to activity data and emission factors, the use of proxy data, poor data, and data gaps ~~Zhang et al. (2023); Zhao et al. (2015)~~(Zhang et al., 2023; Zhao et al., 2015). The uncertainty of anthropogenic Hg emissions is estimated to be especially large for regions where artisanal and small-scale gold mining (ASGM) activities occur ~~Dlamini (2022); Kosai et al. (2023)~~(Dlamini, 2022; Kosai et al., 2023). This is because ASGM often occurs in unregulated or informal contexts, and there is additional uncertainty about the total amount of gold production ~~Yoshimura et al. (2021)~~(Yoshimura et al., 2021). Estimates of emissions from coal-fired power, cement, non-ferrous and gold industrial plants, and waste incineration also vary substantially ~~Cinnirella, S. and Pirrone, N. (2013); Guo et al. (2023); Wang et al. (2021)~~(Cinnirella, S. and Pirrone, N., 2013; Guo et al., 2023; Wang et al., 2021). Emissions estimates from these sectors depend on the Hg concentration and characteristics of the raw material and fuels used, the type of air pollution control device combination applied, and its Hg removal efficiency, all of which are likely to vary significantly between different sources ~~Yang et al. (2016); Kogut et al. (~~(Yang et al., 2016; Kogut et al., 2021; Kwon and Selin, 2016; UNEP, 2017a; Joy and Qureshi, 2023; Wu et al., 2010; Agarwalla et al., 202. Evaluating bottom-up methods across continental areas is challenging because of the presence of local emission sources and atmospheric variability, requiring more frequent and extensive network observations.

Designed to address Hg pollution, the Minamata Convention on Mercury aims to protect human health and the environment from anthropogenic Hg emissions and releases. One of its key provisions is the evaluation of its effectiveness. ~~Different efforts aim to provide scientific support for evaluating the effectiveness of the Minamata Convention on Mercury and the Convention on Long-Range Transboundary Air Pollution.~~ The Multi-Compartment Hg Modeling and Analysis Project, an international collaborative effort, utilizes diverse modeling approaches to examine spatial and long-term changes in environmental Hg ~~Dastoor et al. (2025)~~(Dastoor et al., 2025). One of the scientific efforts aimed at informing the effectiveness evaluation of the Minamata Convention on Mercury ~~have~~ has applied both statistical analyses and process-based modeling techniques to examine trends in mercury monitoring data ~~Feinberg et al. (2024b)~~(Feinberg et al., 2024b). The use of chemical transport models can complement observations, providing a more thorough and detailed understanding of Hg pollution ~~UNEP (2010)~~(UNEP, 2010). The level of agreement between the model simulations and the observed Hg levels is a topic of scientific

~~Travnikov et al. (2017)~~ (Travnikov et al., 2017) and policy interest. Numerous instances can be found in the literature in which model-observation comparison studies have offered new perspectives on the Hg cycle ~~Shah et al. (2021); Feinberg et al. (2022); Ariya et al.~~ (Shah et al., 2021; Feinberg et al., 2022; Ariya et al., 2004; Fisher et al., 2012; Dastoor et al., 2015) and assessed the model capacity to simulate it ~~Feinberg et al. (2024a); Wu et al. (2005); Lindberg et al. (2007); Gabay et al. (2020); Qureshi et al. (2011)~~ (Feinberg et al., 2024a; Wu et al., 2005; Lindberg et al., 2007; Gabay et al., 2020; Qureshi et al., 2011). Observational studies further reveal that model projections can align closely with observations in some regions, while diverging significantly in others ~~Ahmed et al. (2023); Pacyna et al. (2016)~~(Ahmed et al., 2023; Pacyna et al., 2016). Intercomparison studies performed by ~~Travnikov et al. (2017) Travnikov et al. (2017) and Bieser et al. (2017) Bieser et al. (2017)~~ Travnikov et al. (2017) and Bieser et al. (2017) show differences among models in simulated Hg deposition and atmospheric concentrations, even when the same anthropogenic Hg emission inventories are used. Differences in how models treat key processes, such as oxidation pathways and deposition mechanisms can lead to these model-model differences. Despite the identification of these differences, it is often difficult to identify the driving factors behind them (e.g. uncertainties in emissions, chemical processes, or high variability in Hg levels).

The overall dynamics of a global Hg model are complex, and identifying why a model did not match observations in an intercomparison exercise by pointing to a specific model component is difficult ~~Subir et al. (2012)~~(Subir et al., 2012). Model projections are subject to uncertainty arising from various sub-components of the models~~(~~: emissions input characteristics ~~Kwon and Selin (2016); Zyśk et al. (2015); Ryaboshapko et al. (2007); Simone et al. (2016); De Simone et al. (2017); Bullock Jr. et al. (2~~ (Kwon and Selin, 2016; Zyśk et al., 2015; Ryaboshapko et al., 2007; Simone et al., 2016; De Simone et al., 2017; Bullock Jr. et al., 2009) , how chemistry mechanisms are or are not treated ~~Holmes et al. (2010); Zhang et al. (2019); Ariya et al. (2015), meteorological fields Matthias et al. (2013))~~(Holmes et al., 2010; Zhang et al., 2019; Ariya et al., 2015), and meteorological fields (Matthias et al., 2013) . In general, in Hg studies, anthropogenic emissions and other model uncertainties, as well as seasonal and inter-annual variations of Hg levels are discussed and evaluated separately. However, models used for the investigation of emissions uncertainties are also subject to other model uncertainties, and therefore identifying the interactions between different sources of uncertainty is necessary. These model limitations limit the application of models as tools for evaluating Hg mitigation policies and emphasize the need for comprehensive observational networks, improved process representation, and emissions estimations.

Here, we conduct a modeling study that is designed to identify independent signals of anthropogenic emission uncertainties, in the context of other model process uncertainties. Our goal is to identify the extent to which the anthropogenic emissions component of a global model contributes to its ability to reproduce observations, and we apply this analysis to detect areas where additional measurements would improve the evaluation of anthropogenic emission uncertainties. For the representation of anthropogenic emissions uncertainties, we use four different anthropogenic emission estimates. We use the chemical transport model (CTM) GEOS-Chem, which allows in-depth analysis and provides a testbed for comparing the different sources of potential error. Sources of error we evaluate, in addition to multiple estimates of anthropogenic emissions, include two different Hg oxidation schemes, and two different meteorological datasets. Finally, we calculate a signal-to-noise ratio (SNR) measure to identify regions where measurements could better contribute to reducing specific uncertainties.

2 Methods

2.1 Anthropogenic Emission Inventories

The emission estimation methods for the constructed global Hg emission inventories used in this study are detailed in the literature ~~Muntean et al. (2018); Streets et al. (2019); Zhang et al. (2016); Steenhuisen and Wilson (2022, 2019)~~(Muntean et al., 2018; Streets e. Table 1 outlines the global Hg emission inventories considered in this analysis, detailing grid resolution, years of emission inventory, sectoral aggregation used, estimation of uncertainties, and chemical speciation. Chemical speciation refers to the breakdown of chemical forms of ~~the atmospheric~~ emitted Hg into three forms, i.e., gaseous elemental mercury (GEM or Hg^0), gaseous oxidized mercury (GOM or Hg^{2+}), and particulate-bound mercury (PBM or Hg_p) ~~Gustin et al. (2021)~~ (Gustin et al., 2021). The dominant form of Hg in the atmosphere is Hg^0 ($> 95\%$) ~~Mao et al. (2016)~~(Mao et al., 2016), which is the predominant form in the gaseous phase and facilitates global transport. None of the inventories provide information on intra-annual variation of monthly emissions. The AMAP/GMA inventory ~~AMAP/UNEP (2019); Steenhuisen and Wilson (2022, 2019)~~ (AMAP/UNEP, 2019; Steenhuisen and Wilson, 2022, 2019) was developed based on national activity data and national/regional information on emission factors and the efficiency of air pollution control technology. The inventory is built by compiling and geolocating emission point (stacks) sources, as well as identifying the diffuse shares of 21 emission (industry) sectors. The diffuse emissions account for 62.1% of the total emissions, and the spatial proxies used to distribute ASGM emissions significantly affect the sector representation. The EDGAR ~~Muntean et al. (2018)~~ (Muntean et al., 2018) emissions from area (diffuse), line (road and water ways) and point sources are calculated as country-wide totals. EDGAR relies on activity data, emission factors, and control measures information from many data sources such as agencies (e.g. the International Energy Agency (IEA) ~~IEA~~(IEA), the United States Geological Survey (USGS) ~~USGS (2015)~~(USGS, 2015), specialized organizations, treaties, and extended scientific literature ~~UNFCCC (2015); FAO (2015); EMEP/EEA (2013); Artisanal Gold Council (2010); Cement Sustainabili~~ (UNFCCC, 2015; FAO, 2015; EMEP/EEA, 2013; Artisanal Gold Council, 2010; Cement Sustainability Initiative, 2016; Zhao et al., 2008 among others. EDGAR includes road, inland waterways and international shipping as Hg emission sources. The STREETS inventory ~~Streets et al. (2019)~~ (Streets et al., 2019) uses IEA data ~~IEA~~ (IEA) for the fossil fuel combustion sector and considers the use of flue gas desulfurization (FGD) systems in the power sector. For the ASGM sector, the activity levels reported by GMA ~~AMAP/UNEP (2013)~~ (AMAP/UNEP, 2013) were adopted as anchor points for the year 2010 year, using a proxy approach, the emissions for 2010-2015 were estimated. The STREETS inventory obtained data from UNEP ~~UNEP (2017b) and USGS UNFCCC (2015)~~ (UNEP, 2017b) and USGS (UNFCCC, 2015) for industrial metal production and production and use of Hg in commercial products, respectively. The global WHET Hg emission estimate ~~Zhang et al. (2016)~~ (Zhang et al., 2016) is based on the STREETS inventory (and EDGAR for ASGM emissions) and includes updated country-specific estimates for China, India, the US, and Western Europe. The WHET global Hg emission estimate takes into account the application of air pollution control devices (e.g. FGD) in the coal combustion sector in the US that shifts the speciation in emissions. This speciation change in the US is extrapolated to all other countries in North America, Western Europe, and Oceania and was derived by Zhang et al.(2015) ~~Zhang et al. (2015)~~ (Zhang et al., 2015) for China. WHET also takes into account the decline in emissions

from the use and disposal of commercial products based on Horowitz et al.(2014) ~~Horowitz et al. (2014)~~(Horowitz et al., 2014) .

Fig. 1 shows the latitudinal profiles of the annual anthropogenic Hg emissions (Mg y^{-1}) and the spatial distribution of the TGM emissions range from the different inventories. Figure 2 presents the differences in emissions (Mg y^{-1}) ~~between~~ among the four different inventories by species and continent (in approximation using box masks). The percentage of emissions located in the Northern Hemisphere varies from 77.6% to 88.5% for the different inventories. There are multiple regions in Northern Canada, Alaska, the Sahel, northern Russia, and Australia where some inventories document zero emissions, ~~as opposed to others~~ and others report emissions. A comparison of inventories reveals large differences in Asia in terms of GOM and PBM emissions. Differences in GEM emissions are also pronounced in Asia, South America, and Africa. The overall chemical composition ratio GEM:(GOM+PBM) ranges between 1.83 and 4.57 for the different inventories.

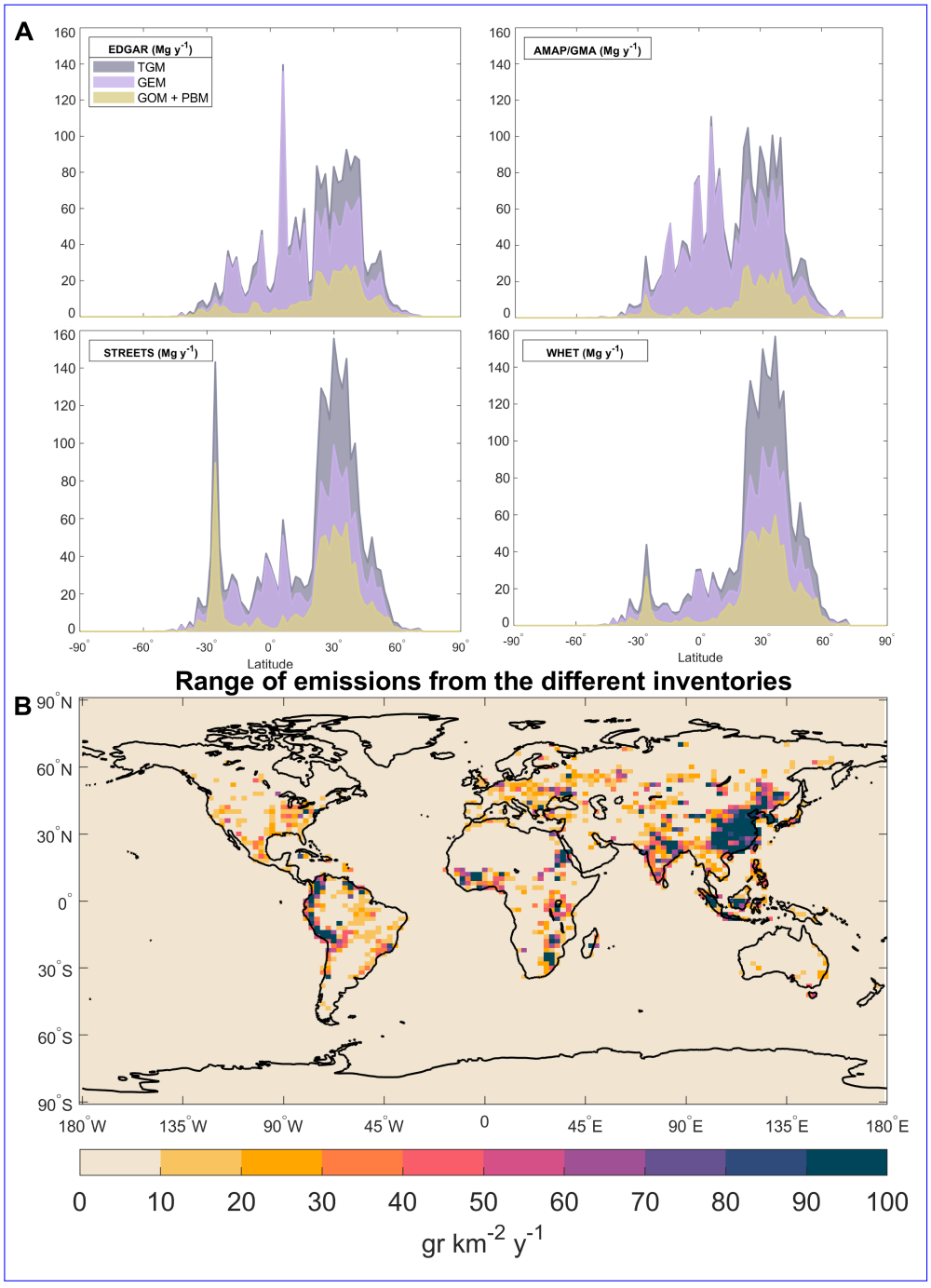

Figure 1. a) shows the latitudinal profile of annual Hg anthropogenic emissions (Mg y^{-1}) and b) the spatial distribution of the range of TGM emission from the different inventories and global emission estimates (~~gr~~ g km^{-2} y^{-1}). The inventories correspond to different representative years: EDGAR (2012), AMAP/GMA (2015), STREETS (2013–2015), and WHET (2010).

Table 1. Overview of Hg anthropogenic emission inventories used in this study. The uncertainty ranges refer to reported uncertainties in global total anthropogenic Hg emissions for each inventory, as provided by the original sources.

Inventory	Grid Resolution	Years	Available sectoral emissions	Species	Uncertainty	References
AMAP/GMA	0.25°×0.25°(2015)	1990-1995, 2000-2010, 2015	Power generation, Industrial sources, Intentional use and product waste, ASGM (2015)	GEM, GOM, PBM	−20∼68%	(Steenhuisen and Wilson, 2022)
EDGAR	0.1°×0.1°	1970-2012	Cement manufacturing, chlor-alkali production, combustion in the power sector and industry, combustion in residential and other sectors, glassmaking, ASGM, Large-scale gold production, iron production, non-ferrous and other metal production, shipping, road transportation, waste incineration	GEM, GOM, PBM	−26∼33%	(Muntean et al., 2014), (Muntean et al., 2018)
STREETS	1°× 1°	2000-2015	All sector totals which include: fossil fuel combustion, industrial metals production, ASGM and production and uses of Hg in commercial products.	GEM, GOM, PBM	−20∼44%	(Streets et al., 2009), (Streets et al., 2019)
WHET	1°× 1°	1990, 2000, 2010	All sector totals which include: ASGM, Combustion, and Products	GEM, GOM, PBM	−33∼60%	(Zhang et al., 2016)

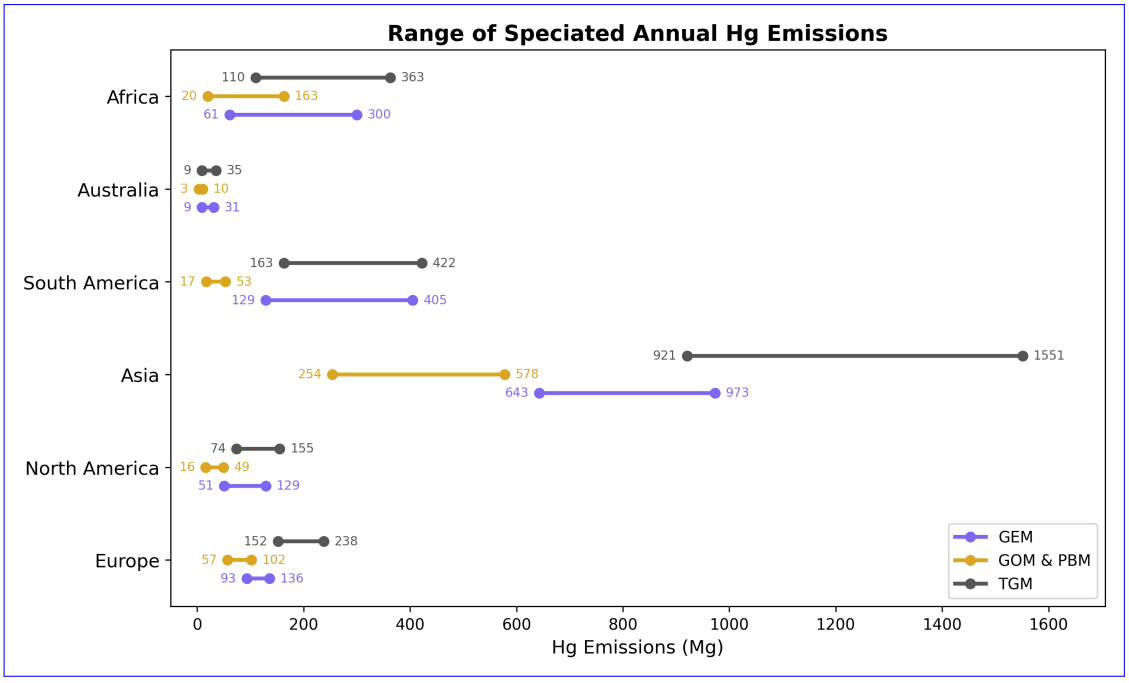

Figure 2. Range of speciated annual Hg emissions (in Mg) by continent, based on estimates from four different inventories. The inventories correspond to the following representative years: EDGAR (2012), AMAP/GMA (2015), STREETS (2013–2015), and WHET (2010).

2.2 Model and simulations

We used the GEOS-Chem model (v 12.8.01) (www.geos-chem.org) for the Hg simulation ~~Horowitz et al. (2017)~~ (Horowitz et al., 2017) to estimate the effect of different uncertainties in modeling results at a horizontal resolution of 2 ° latitude by 2.5 ° longitude

and 47 vertical levels. GEOS-Chem is driven by the assimilated meteorological MERRA-2 dataset and is parallelized using OpenMP. The simulations included three Hg tracers: GEM, GOM, and PBM. Both primary emissions and secondary re-emissions from soil and snow are included ~~Selin et al. (2008)~~(Selin et al., 2008). The snow re-emissions are tied to solar radiation, and the re-emission rate used is based on the study of ~~Durnford and Dastoor (2011)~~Durnford and Dastoor (2011) Durnford and Dastoor (2011). Legacy Hg reemissions from the ocean were archived from the MITgcm model ~~Horowitz et al. (2017)~~ (Horowitz et al., 2017), and monthly Br fields were taken from full-chemistry GEOS-Chem simulations ~~Schmidt et al. (2016)~~ (Schmidt et al., 2016), respectively. Surface–atmosphere Hg exchange processes, including soil, snow, and ocean re-emissions, are included in GEOS-Chem but are prescribed independently of the anthropogenic emission inventory used in each simulation. As a result, differences among anthropogenic emission inventories do not propagate into inventory-specific legacy re-emissions. This modeling choice allows isolation of the atmospheric uncertainty attributable to inventories of direct anthropogenic emissions. The atmospheric GEM oxidation mechanism considers gas-phase Br as the primary oxidant in the troposphere and stratosphere, and second-stage oxidation of HgBr by a number of radical oxidants ~~Horowitz et al. (2017)~~(Horowitz et al., 2017). For half of the simulations, we used an alternative GEM oxidation mechanism ~~Selin et al. (2008)~~ (Selin et al., 2008) where the predominant oxidants are OH and O_3. ~~The oxidant fields were computed from a GEOS-Chem full chemistry simulation. While the OHand O_3 scheme includes reactions which previous studies Castro et al. (2022) have judged unlikely to occur at given rates in the atmosphere , its implementation here allows us to proxy chemical uncertainty~~More advanced chemical mechanisms have since been developed which incorporate the oxidation of Hg^0 of both OH and Br, followed by oxidation by O_3 in a second-step (Castro et al., 2022; Shah et al., 2021; Saiz-Lopez et al., 2020, 2025). Nevertheless, by conducting two sets of simulations with radically different chemistry schemes (Br vs. OH/O_3), we can identify which regions of the atmosphere are most affected by chemical uncertainties. The model also calculates spatial fields of wet deposition of GOM and PBM consisting of scavenging in wet convective updrafts and rainout and washout in large-scale precipitation ~~Liu et al. (2001)~~ (Liu et al., 2001) and dry deposition of all three species. GEOS-Chem uses a formulation consistent with a resistance-based GEM dry deposition ~~Travnikov et al. (2017)~~(Wesely, 1989).

Our model experiments (Table 3) are designed in three groups to compare the magnitudes of model uncertainties driven by anthropogenic emissions, chemistry, and meteorological data. Each group was constructed by varying one input while holding others constant to isolate its influence on model output. To assess anthropogenic emissions uncertainty, we conducted the *Inventories* simulations, consisting of four simulations with the Br oxidation scheme, each utilizing a different inventory of anthropogenic emissions. To evaluate chemistry uncertainty, the *Chemistry* simulations comprise eight simulations. This group includes four simulations using the Br oxidation scheme, each with a different inventory of anthropogenic emissions, as well as four simulations utilizing the OH/O_3 oxidation scheme, which are also based on different inventories of anthropogenic emissions. ~~However, our~~ These simulations aim to highlight potential differences resulting from the selection of chemical mechanisms, clarifying their contribution to modeled atmospheric processes. The output variables from each set of simulations were averaged to obtain their means, which were then compared to represent the chemistry uncertainty. A 2-year spin-up period was used for the *Inventories* and *Chemistry* simulations and the results from the third, fourth, and fifth years, 2013, 2014, and 2015, were used for the analysis as a multi-annual mean (2013-2015). For the *Meteo* simulations group, we ran the model

twice for the year 2015 using the Br oxidation scheme and the AMAP/GMA emission inventory, each time based on a different meteorological dataset: MERRA-2and GEOS-FP.

2.3 Measurements

GEM observations are obtained from the compilations of ~~Travnikov et al.Travnikov et al. (2017)~~ Travnikov et al. (2017) (courtesy of Hélène Angot) and AMAP/UNEP ~~AMAP/UNEP (2019). The GOM~~ (AMAP/UNEP, 2019). The wet deposition flux observations are compiled by ~~Travnikov et al.Travnikov et al. (2017)~~ Travnikov et al. (2017) (courtesy of Hélène Angot), ~~Sprovieri et al.Sprovieri et al. (2017)~~Sprovieri et al. (2017), AMAP/UNEP ~~AMAP/UNEP (2019) and Fu et al. Fu et al. (2016).~~ (AMAP/UNEP, 2019 and Fu et al. (2016). In this study, only observations collected between 2013 and 2015 are included.

2.4 SNR as a measure for extracting a model's uncertainty effect size under intra-annual variability

SNR compares the level of a signal of interest with the level of background noise ~~Welvaert and Rosseel (2013)~~(Welvaert and Rosseel, 2013) . There is a substantial body of research that has used the SNR measure in atmospheric sciences ~~Acosta Navarro and Toreti (2023); Doi et al~~ (Acosta Navarro and Toreti, 2023; Doi et al., 2022; Yu et al., 2020; Hamilton and Hart, 2023; Hasselmann, 1979; Falkena et al., 2022) . In our study, the SNR is used to identify regions where the model-observation studies are suitable for the evaluation of anthropogenic emissions uncertainty. In this case, the signal is defined as the range (maximum minus minimum) of the model output variable across all simulations within a group (e.g., Inventories, Chemistry, or Meteo). The noise is quantified by first calculating the temporal standard deviation of the model output for each individual simulation, and then averaging those standard deviations across all simulations in the group. This average represents the typical intra-annual variability used in the denominator of the SNR. A high SNR indicates a large signal (high propagated uncertainty to modeling results) compared to the noise (relatively small intra-annual variability). We apply SNR to modeled atmospheric Hg concentrations and wet deposition output to extract the signal due to anthropogenic emissions and other model uncertainties in the presence of intra-annual variability. We use the SNR as defined by the following equation:

$$SNR = \frac{\text{range across simulations in a group}}{\text{average of temporal STDs within each simulation}} = \frac{\max(x_i) - \min(x_i)}{\frac{1}{n}\sum_{i=1}^{n} \sigma_t(x_i)}$$

where:

- x_i is the output variable from simulation i
- $\sigma_t(x_i)$ is the temporal standard deviation for that simulation
- n is the number of simulations in the group

The range within each of the three simulation groups provides a representation of the uncertainties that arise from emissions, chemistry, and meteorology, respectively. We used the mean annual daily standard deviation (STD) as a direct measure of ~~TGM~~GEM, and weekly STD for wet deposition intra-annual variability. We used a weekly time frame for wet deposition because observation samples were collected on a weekly basis.

3 Results

3.1 SNR of major Hg modeling uncertainties

3.1.1 Stations' locations

We analyzed ~~TGM data from 43~~ GEM data from 34 monitoring stations (Fig. 3~~and S. I. Fig.S1~~, Fig. A1 and Fig.A5) aggregated in 6 wider regions and compared them with the variability in modeling results for the three different simulation groups (*Inventories*, *Chemistry*, and *Meteo*). The variability in the model output resulting from the emission input set is larger in four of the six regions (Asia, the United States, Europe, and the Arctic Circle) compared to the variability caused by chemistry or meteorology input sets. The effect of the meteorological data choice does not lead to considerable differences in the modeled ~~TGM~~ GEM in any region.

In Asia (Fig. ~~2~~3, A, D, G), the impact of the Hg oxidation pathway on modeled ~~TGM~~ GEM is minimal, while the *Inventories* simulations group shows a range of up to ≈ 0.3 ng m^{-3}. However, the range of the modeled ~~TGM~~ GEM is not as pronounced as the variability in the observed ~~TGM~~ GEM between different stations and days. Based on the inventories used in this study, Asia is the ~~largest emitter~~region with the largest emissions, contributing 51.5 - 68.9 % to global anthropogenic Hg emissions. The high level and spatial and temporal variability of observed ~~TGM~~ GEM (Fig. ~~2~~ 3 A and G) indicate numerous continuous and episodic high-emitting sources.

In the Arctic, the range of simulated ~~TGM~~ GEM in the *Inventories* simulations group is below the observations' range. A possible explanation is that, as the Arctic is primarily a receptor region, the long-range transport of Hg to the Arctic may be underestimated, or that sources contributing to Arctic Hg may be underestimated in current emission inventories. Several studies point to Asia, Europe, and North America as the main contributors to Hg concentrations in the Arctic ~~Dastoor et al. (2022b); Durnford et al. (2010)~~(Dastoor et al., 2022b; Durnford et al., 2010). As can be seen in Table 2, the annual GEM emission estimates differ by 330.5 Mg in Asia, 43.2 Mg in Europe, and 78 Mg in North America. In addition to the diversity in anthropogenic emissions inventories that lead to a wide range of RMSE for the *Inventories* simulations group, the RMSE reaches its highest point during the summer months. Although the model captures most of the seasonal effects, it is not capable of simulating the peak in ~~TGM~~ GEM levels during the summer. A considerable amount of literature has been published on the maximum ~~TGM~~ GEM concentration levels observed in summer, which are attributed to snow and sea ice melt and oceanic Hg reemissions ~~Dastoor et al. (2022b); Ahmed et al. (2023); Huang et al. (2023); Araujo et al. (2022); Dastoor et al. (2022a)~~ (Angot et al., 2016a; Araujo et al., 2022; Huang et al., 2025; Yue et al., 2023).

In the Southern Hemisphere (SH midlatitudes, Antarctica and Australia regions), the chemistry scheme used to simulate ~~TGM~~ GEM contributes more variability than the emissions inventory used (Fig.~~2~~ .3 C and F). Recent findings indicate an atmospheric Hg lifetime of 3 to 6 months ~~Shah et al. (2021); Horowitz et al. (2017); Zhang and Zhang (2022)~~(Shah et al., 2021; Horowitz et al., , which means that Hg ~~functions primarily as a pollutant on the hemispheric scale Driscoll et al. (2013)~~emissions remain in the hemisphere of origin (Driscoll et al., 2013). A previous study of Hg source-receptor relationships using GEOS-Chem ~~Corbitt et al. (2011)~~ (Corbitt et al., 2011) found that extra-tropical sources have a particularly strong influence on regions within

their own hemisphere. The anthropogenic emission inventories used in this study account for only 11.5% to 22.4% of global emissions located in the Southern Hemisphere, partially explaining their limited influence on model error analysis. The SH mid-latitude region includes Cape Point, Amsterdam Island, and Bariloche sites. Cape Point and Amsterdam Island are marine sites greatly influenced by the ocean ~~Angot et al. (2014); Schneider et al. (2023); Slemr et al. (2020)~~(Angot et al., 2014; Schneider et al., 2023;
. Given that 81% of the Southern Hemisphere surface is ocean ~~Schneider et al. (2023)~~(Schneider et al., 2023), air-sea exchange processes are an extremely important component in the Hg cycle in this hemisphere ~~Bieser et al. (2020)~~(Bieser et al., 2020). The choice of Hg oxidation scheme leads to a significant impact in the modeled ~~TGM~~ GEM in the Southern Hemisphere, as a result of the different distributions of Hg(0) oxidation and the chemical lifetime of tropospheric GEM.

3.1.2 Global

Model error signals can be obscured by noise in model-observation comparisons. To identify the extent of model error signals embedded in the background 'noise' of natural variability, we examine the SNR. Fig. 4 A illustrates the global annual daily-averaged STD of simulated ~~TGM~~ GEM for the group *Inventories*. The model estimated a markedly high intra-annual variability of ~~TGM~~ GEM in areas characterized by exceptionally high emission levels, such as South and East Asia, which is also observed on a monthly basis through observations (Fig. 3 G). A high intra-annual variability of ~~TGM~~ GEM is found in Antarctica and generally in more southern latitudes as corroborated by the S.I. Fig. 1 and several publications ~~Pfaffhuber et al. (2012); Temme et al. (2003); Dommergue, A. et al. (2013); Dommergue et al. (2010); Sprovieri et al. (2002)~~(Angot et al.
. The global map in Fig. 4 B displays the annual weekly-averaged STD of wet deposition. STD of wet deposition is high over the oceans and is also evident in some regions of eastern North America and South America.

The results obtained using the SNR analysis of the ~~TGM~~ GEM model outputs for the *Inventories* and *Chemistry* simulations groups are illustrated in Fig. 4 C and D. For the Group *Meteo*, the Figure ~~S4~~ A4 shows SNR greater than 1 for ~~TGM~~ GEM only over the equatorial western part of South America. The SNR patterns for simulation groups *Inventories* and *Chemistry* are largely anti-correlated, with values exceeding 1 in one group typically corresponding to lower values in the other. Annually averaged ~~TGM~~ GEM measurements in the Northern Hemisphere provide an optimal and independent constraint for evaluating uncertainties in anthropogenic emission inventories, distinct from other uncertainty signals considered in this study. The U.S. Atmospheric Mercury Network (AMNet), particularly the eastern zone, constitutes one of the most reliable monitoring systems for the Hg emission inventory assessment using ~~TGM~~ GEM measurements. However, even though there are numerous stations located in areas with high SNR during winter months, the monitoring networks remain spatially limited, resulting in insufficient coverage of areas with high SNR, including Greenland, the Mediterranean Sea, Arctic Russia as well as regions in South America, and Africa. In contrast, relatively continuous ~~TGM~~ GEM measurements in the mid- and high-latitude regions of the Southern Hemisphere are better suited to isolate and assess uncertainties in the chemical mechanisms, as these regions exhibit low SNR for anthropogenic emissions and pronounced impact of chemical scheme choices ~~.~~(Fig. 4 D).

Figure 4 E and F depict the results derived from the SNR analysis applied to the wet deposition model outputs for the *Inventories* and *Chemistry* simulations groups. Figure ~~S4~~ A4 presents the SNR for wet deposition in the Group *Meteo*, indicating a moderate signal strength in wet deposition in the Southern Hemisphere. The SNR measure illustrates that wet

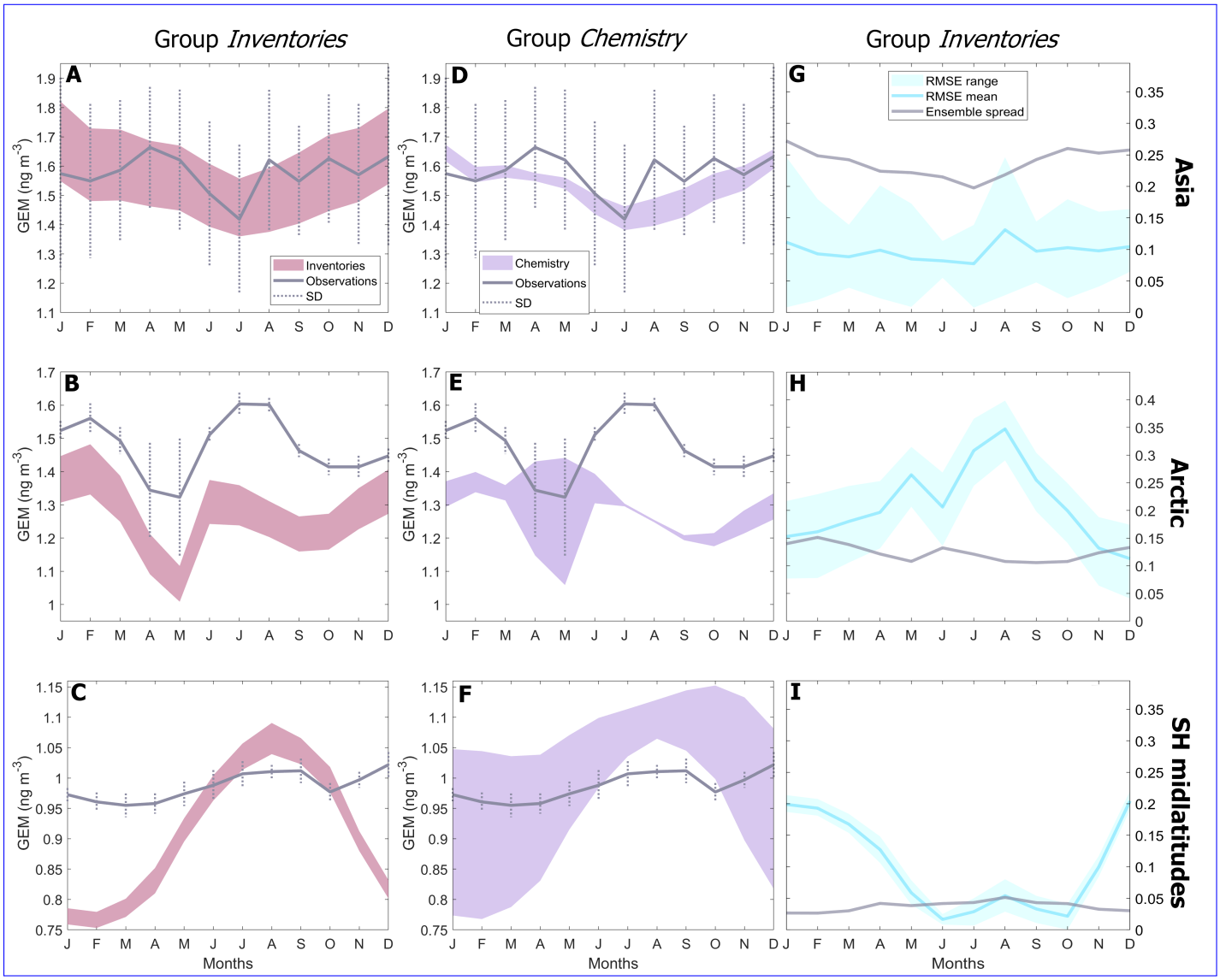

Figure 3. Seasonal variation of ~~TGM~~ GEM (monthly averages and their STD among stations) for stations located in the Arctic, Asia and Southern Hemisphere mid-latitudes. The range of the simulated ~~TGM~~ GEM is depicted in pink (A-C) and purple (D-F), respectively for the *Inventories* simulations group and *Chemistry*, respectively. The third column (G-I) shows the calculated RMSE range and mean, and the group range~~, the daily monthly averaged STD of TGM (model and observations)~~.

deposition measurements are less sensitive to the change in anthropogenic emissions within the *Inventories* simulations group (Fig. 4 E), as compared to ~~TGM~~ GEM measurements (Fig. 4 C). Nonetheless, there exist specific regions where the SNR attains a value of 1, with some of these locations also coinciding with monitoring stations (East Asia). On the other hand, the SNR pattern of the ensemble *Chemistry* reveals strong signals throughout the globe except in the subtropical areas. Several studies

have identified errors or gaps in the chemical mechanisms related to the atmospheric oxidation of GEM, which is a critical precursor to both wet and dry deposition processes ~~Wang et al. (2014); Skov et al. (2004)~~(Wang et al., 2014; Skov et al., 2004) . The SNR for wet deposition in the group ~~MEteo~~ *Meteo* indicates a wider moderate SNR in wet deposition throughout North America, Europe, and South Asia.

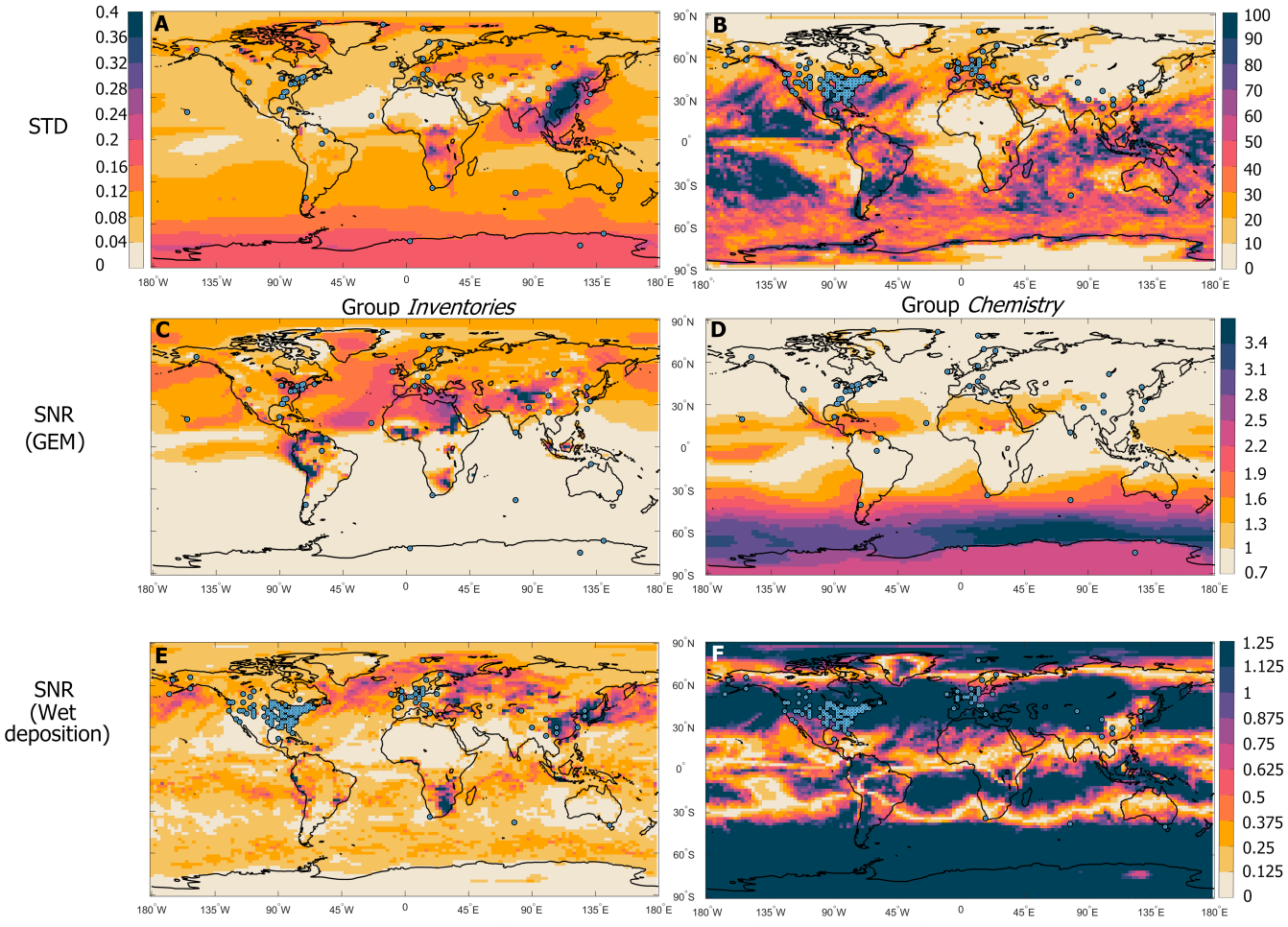

Figure 4. Spatial distribution of the daily monthly averaged STD of ~~TGM~~ GEM (ng m^{-3}) (A) and annual weekly-averaged STD of wet deposition (ng m^{-2}) (B). SNR of ~~TGM~~ GEM and wet deposition when using: different inventories (C, E) and different chemistry schemes (D, F).

3.1.3 Seasonality

Figure 5 presents the SNR pattern over the globe for different seasons. While the SNR is consistent over seasons in some regions, in others, the SNR demonstrates seasonal variation, controlled by seasonal patterns such as meteorological conditions and atmospheric chemistry. The Mediterranean Sea, eastern U.S., and eastern Russia do not show significant seasonal changes in the SNR, making them ideal regions for observationally-based emission evaluation throughout the year. For the Arctic and northern Eurasia, the winter months have a higher SNR. Winter is the most promising period to evaluate emission uncertainties through ~~TGM~~ GEM background concentrations in the Arctic, as it is not influenced by local chemical processes that could introduce sources of noise (e.g. AMDEs ~~Steffen et al. (2008); Skov et al. (2020)~~(Steffen et al., 2008; Skov et al., 2020)). In the central and western U.S., the decrease in SNR in autumn is likely due to increased ~~TGM~~ GEM anomalies caused by meteorological factors ~~Xu et al. (2022)~~(Xu et al., 2022). In Europe and central Eurasia, the response of modeled ~~TGM~~ GEM on emissions uncertainty is higher during the winter. However, the model results suggest low STD of ~~TGM~~ GEM during the summer resulting in a high SNR (Fig. 5 C).

Even ~~at an intra-annual level~~intra-annually, the signal of emissions uncertainties rarely exceeds the noise (Fig. 5 E-H) in modeled wet deposition. In particular, Australia and South America ~~give~~ have very low SNR values. The low signal and high variability of modeled wet deposition indicate that they hamper the evaluation of emissions uncertainties or even hide anthropogenic emissions effects on wet deposition. The exception is in northeast Asia, where the detection capability of emissions uncertainty on modeled wet deposition appears to be >1 throughout the year. In contrast to the SNR based on the modeled ~~TGM~~GEM, the SNR based on the wet deposition is greater than 1 in spring and autumn in the Arctic (Fig. 5, F, H). The extended spatial spread of SNR greater than 1 in the Arctic during the autumn results from a low STD of wet deposition of Hg. This means that measuring wet deposition and assessing emissions in autumn could give insights into the northern hemispheric background Hg. In the springtime, in the Arctic and in Central North Russia, isolating the emissions uncertainty signal in spring is more efficient.

3.2 Discussion

CTMs are typically evaluated based on their performance in simulating atmospheric Hg concentrations and deposition. In contrast, this study focuses on assessing how modeling choices affect the robustness of CTMs when used to evaluate anthropogenic Hg emission inventories. As the bottom-up method for Hg emission estimation suffers from various uncertainties and the current anthropogenic Hg inventories differ by substantial amounts, independent constraints from observations could shed light on primary anthropogenic Hg emissions uncertainties. Our simulations generate insight into which sites could provide or not the most relevant constraints on primary anthropogenic Hg emissions.

This modeling experiment reveals that different regions of the world exhibit varying levels of sensitivity to model components, such as emissions and atmospheric chemistry. The large differences in anthropogenic emissions estimates for Asia dominate the variability in modeled ~~TGM~~GEM. However, ~~this~~ when considering aggregated monitoring sites across Asia, the resulting discrepancy in modeled ~~TGM in Asia cannot~~ GEM may not always be easily constrained by model-observation

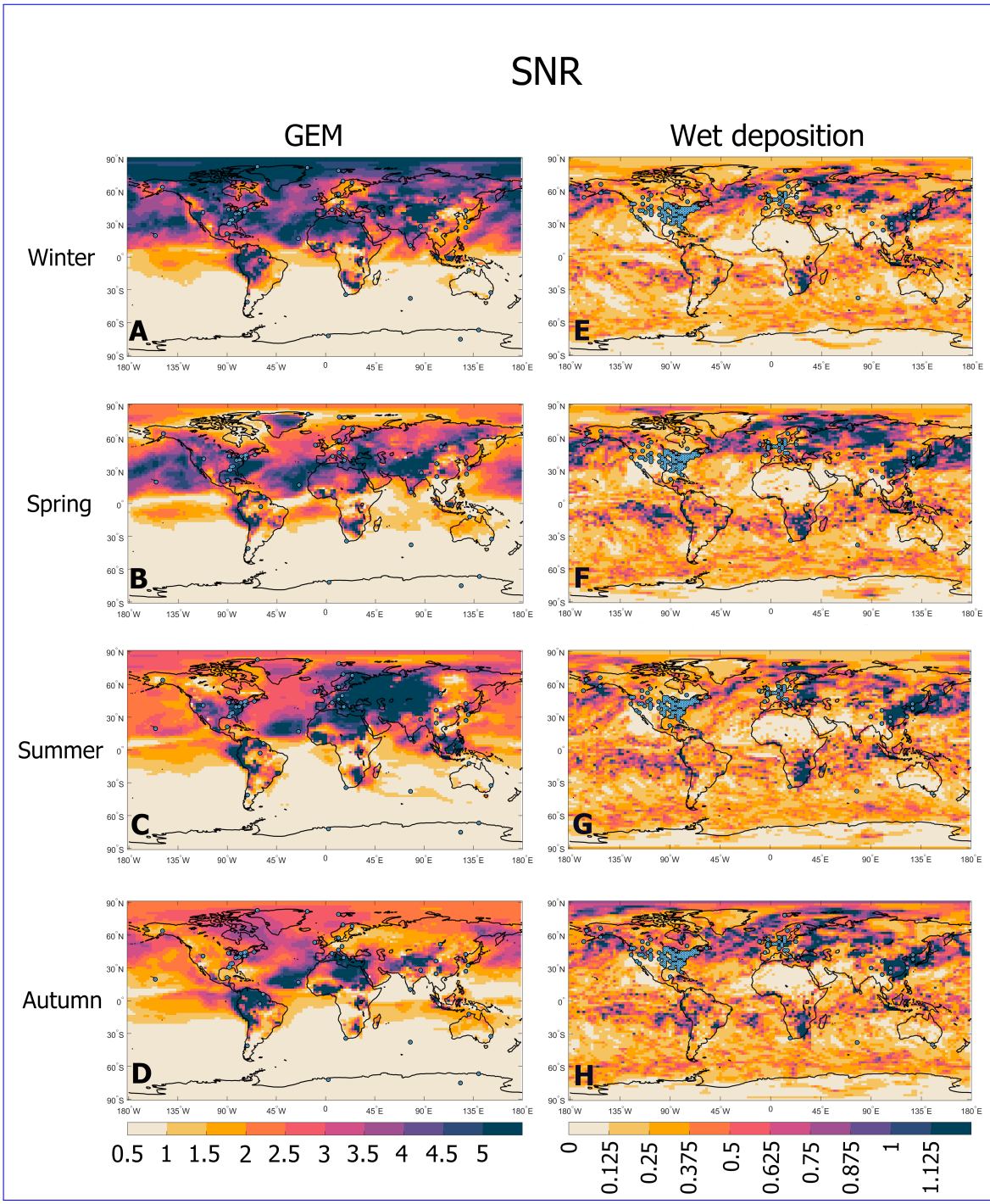

Figure 5. Seasonality of SNR of: ~~TGM~~ GEM (left) and wet deposition (right) for the Group *Inventories*.

comparisons using the current observation sites. The reason is that, in this case, the range of the model results falls within the range of ~~TGM~~ GEM measurement variability (Fig 3 ~~, A)and this fact adds further challenges in evaluating anthropogenic emissions uncertainty~~A), which partly reflects spatial aggregation of heterogeneous monitoring locations. The spatial SNR patterns shown in Fig. 4C highlight subregional differences. For example, central China and Central Asia exhibit relatively high SNR values, whereas eastern China shows lower SNR. While the largest absolute uncertainties in anthropogenic Hg emissions occur in Asia and South America, our analysis identifies regions where background observations are most effective at isolating emission signals from other sources of variability, which is a distinct but complementary objective.

Based on our modeling results, we show that current SH monitoring networks are not ideal to help evaluate anthropogenic emissions uncertainties, but they could be instrumental in addressing uncertainties related to chemical processes. Current observations in the SH are insufficient to evaluate anthropogenic emissions uncertainties due to distances from areas with positive SNR (apart from the Nieuw Nickerie and Manaus sites) and their limited spatial coverage (Fig. 4 C). The majority of ~~TGM~~ GEM observation sites in the SH are located in areas where chemistry uncertainty and intra-annual variability completely impede detection signals of anthropogenic emissions uncertainty. For instance, when analyzing the annual averaged results for the SH mid-latitudes and Antarctica, the response of the model across different emission inventories remains below 0.06 ng m^{-3} and 0.04 ng m^{-3} range of ~~TGM~~GEM, respectively. The low sensitivity to the different inventories in conjunction with up to 0.2 ng m^{-3} intra-annual variability of ~~TGM~~ GEM leads to very low SNR across much of the Southern Hemisphere monitoring network. However, this result should not be interpreted solely as evidence of a true physical insensitivity of Southern Hemisphere Hg concentrations to anthropogenic emissions. The weak emissions SNR may also reflect limitations in currently available anthropogenic Hg emission inventories for the Southern Hemisphere, where emissions from ASGM and industrial sources are known to be poorly constrained (AMAP/UNEP, 2019). Future studies could address this point using new emissions inventories that have been published after these simulations were completed (Qiu et al., 2025; Muntean et al., 2024; Cui et al., 2025; MacFarlane et al., 2022). In this context, a low SNR may arise from an under-representation or misallocation of anthropogenic emissions in the input data. Improved bottom-up emission estimates and enhanced observational coverage in the Southern Hemisphere could therefore improve the ability of monitoring networks to constrain anthropogenic Hg emissions uncertainties.

The chemistry and meteorological data model settings and the intra-annual Hg variability have less impact on model-simulated Hg concentrations and wet deposition in Europe, the USA, and the Arctic. The model and the observations agree that the STD of ~~TGM~~ GEM for the Arctic Circle (Fig. 3, H), USA (Fig. ~~S1~~A1, I), and Europe (Fig. ~~S1~~A1, H) monitoring systems is low (smaller than 0.09 ng m^{-3}) for any month of the year. Distinguishing emissions uncertainty signals over intra-annual variability of ~~TGM~~ GEM in the sites of the Arctic Circle is feasible, as the former is more than twice as large as the latter. In winter, SNR exceeds the value of 5.5 in both Greenland sites. Similarly, sites that could help constrain the uncertainties of anthropogenic emissions are those in South Europe and the East US. While the SNR analysis identifies regions such as the Arctic and specifically Arctic Russia, Greenland, as theoretically optimal for isolating anthropogenic Hg emission signals—particularly during winter—these findings should be interpreted in the context of substantial real-world constraints. Harsh environmental conditions, including extreme cold, prolonged darkness, snow and ice cover, and limited accessibility,

pose significant operational challenges for sustained monitoring in the Arctic. In addition, strengthening monitoring coverage in remote areas such as Greenland and Arctic Russia faces logistical, infrastructural, and geopolitical constraints.

Studies of Hg emissions and atmospheric processes that are performed using a single model present advantages but also limitations. One advantage of employing one model is that it allows a controlled and consistent framework to systematically evaluate specific uncertainties, such as those arising from emission inventories, chemical mechanisms, or meteorological datasets. With this approach, it is possible to focus on specific sources of modeling uncertainty and derive more accurate conclusions within a specific, invariant model architecture. Additionally, an experiment with a single model often reduces computational costs and complexity, facilitating performing a group of simulations within a consistent modeling environment. Despite its benefits, this method entails certain limitations. A single model inherently reflects the biases and limitations of its design, such as its specific treatment of Hg chemistry or resolution constraints. Such biases may result in overconfidence in findings, which might not apply to other models. On the other hand, multi-model studies enable exploration of the diversity of outcomes, which commonly improve the robustness of the analysis of uncertainty and confidence in predictions. To address this issue, our study incorporated two fundamentally different chemistry schemes, representing distinct oxidation pathways (Br and OH/O_3-based chemistry), within the same modeling framework. Using these different chemical schemes allowed us to cover a broad range of chemical uncertainties and reduce the potential for bias linked to dependence on a single chemical mechanism. Future studies could conduct similar ~~analyses~~ analysis using other global mercury models ~~and different chemistry schemes Shah et al. (2021); Dastoor et al. (2025)~~(Dastoor et al., 2025), as well as updated Hg chemistry schemes (Saiz-Lopez et al., 2025; Shah et al., 2021).

One limitation of the present analysis is that inventory-dependent re-emissions are not represented. The modeled response to anthropogenic emission differences likely underestimates the full influence of emissions on atmospheric Hg. Such an approach is beyond the scope of the present work and would complicate attribution of modeled atmospheric differences to specific sources of uncertainty. Therefore, our results should be interpreted as a lower-bound estimate of the relative importance of anthropogenic emission uncertainties compared to chemistry and meteorology. Additionally, the *Meteo* simulations are intended to assess sensitivity to commonly used assimilated meteorological datasets within the GEOS-Chem framework rather than to represent the full range of meteorological model uncertainty.

To effectively reduce anthropogenic Hg emission estimate uncertainties and support global Hg policy goals, the design of Hg monitoring networks could better target regions with high SNR of anthropogenic emissions uncertainties and minimal overlapping signals from multiple other sources (e.g., chemistry, and meteorology). The eastern U.S., Greenland, and Arctic Russia (Fig. 4, C), are ideal locations for year-round monitoring to evaluate the potential uncertainties of anthropogenic Hg emission inventories. Such regions with high SNR can effectively minimize background noise and isolate clear signals of anthropogenic Hg emissions. For example, the whole Arctic's high SNR during winter months (Fig. 5) makes it an excellent location for studying Northern Hemisphere background Hg concentrations, independent of other chemical or meteorological errors in modeling results (Fig. 4, D and ~~S4~~A4). Additionally, regions like Eurasia, northern Canada, and central North America show high SNR during specific seasons (Fig. 5), making them key areas for detecting emissions uncertainty, particularly in seasons when Hg transformation or deposition processes are more stable.

Key regions for intensive monitoring include high-emission regions such as Asia, South America, and Africa, where ASGM and industrial activities prevail. With China and India producing high industrial, and coal combustion Hg emissions, Asia is the biggest emitter ~~AMAP/UNEP (2019)~~(AMAP/UNEP, 2019). Identifying and quantifying such sources of high emission remains a major challenge, and an enhanced strategy and dense monitoring are needed to reduce associated uncertainties. Monitoring stations could be densely distributed in these regions to capture the full range of emissions and their shifts in space and time (Fig. 2, A, D, G) and better estimate anthropogenic Hg emissions. The main sources of emissions in South America and Africa are ASGM, fuel combustion, and industrial activities ~~AMAP/UNEP (2019) requiring~~ (AMAP/UNEP, 2019), and targeted monitoring strategies are necessary to address the significant uncertainties in Hg emissions from these activities. Large portions of the globe remain undersampled, including parts of Africa, South America, and Asia. Measurements in these areas are important for improving the understanding of Hg sources. Expanding the global monitoring network would complement observations in high-emission and high-SNR regions and strengthen model–observation comparisons used to evaluate Hg emissions and atmospheric processes. In addition, tailored wet deposition monitoring in regions like Asia and South Africa, where emission estimates vary widely, is essential to constraining emissions, as the high SNR suggests strong potential to constrain model uncertainties (Fig. 3, E). Although enhanced wet deposition monitoring in regions such as South Africa may be informative from a modeling perspective, such recommendations must be considered alongside regional climatology. Much of southern Africa is characterized by arid or semi-arid conditions and recurrent droughts, limiting the feasibility and interpretability of continuous wet deposition measurements.

In addition to high-emission zones, remote receptor regions, such as the Arctic, are instrumental in capturing long-range Hg transport and deposition. The Arctic, as a receptor region, is of considerable importance in understanding global Hg transport, especially from major emitting regions such as Asia, Europe, and North America. However, current modeling underestimates ~~TGM~~ GEM in this region (Fig. 3, B, E, H), making it imperative to enhance ~~new~~ monitoring efforts in Greenland and Arctic Russia (Fig. 4, C). Monitoring in these remote locations will provide baseline data to shed light on the causes of model-observation discrepancies as well as anthropogenic emission uncertainties.

Observations should be consistently used in model–observation comparison studies with CTMs such as GEOS-Chem to ensure that the monitoring network provides actionable insights for policy-makers and the Minamata Convention on Mercury. In this way, refinement of Hg emission estimates would be possible, especially in regions where significant discrepancies exist between observed and modeled data. The benefits of using inverse modeling techniques ~~Song et al. (2015)~~ (Song et al., 2015) are also important in constraining emission inventories based on observations. Inverse modeling refines Hg emission estimates by adjusting model inputs to better match observations like ~~TGM~~ GEM or wet deposition. Using models such as GEOS-Chem, emissions are iteratively optimized to minimize differences between simulations and observations. This top-down approach is especially useful to identify and correct inventory biases. Therefore, strengthening the monitoring network would not only enhance our understanding of the Hg global distribution and deposition but also provide critical data to guide future policy interventions aimed at reducing global Hg emissions.

For the Hg modeling community, this study points to the importance of addressing both emissions and other model uncertainties simultaneously rather than in isolation. The complex interactions between emission inputs, chemical processes,

and meteorological data require models to be tested holistically. As demonstrated in this work, emission uncertainties could mask the impacts of other model errors regarding Hg wet deposition (Central America, Fig. 4, C, D), and vice versa. Therefore, to minimize overall uncertainty, model developers and users should not only improve the accuracy of emission input data but also refine the representation of key atmospheric processes within models, such as Hg oxidation and deposition mechanisms. This dual approach is essential because, as shown in this study, uncertainties in emissions and chemistry can interact and amplify total model uncertainty in complex ways.

4 Conclusion

This study offers a better understanding of the role of anthropogenic Hg emission uncertainties in the performance of global Hg models, underscoring the need for more precise emission inventories and monitoring strategies for their evaluation. We have demonstrated that differences among emission inventories, particularly in high-emission regions like Asia, can introduce significant differences in modeled ~~TGM~~ GEM concentrations, especially in the NH, with regional discrepancies across modeling results reaching up to 0.47 ng m^{-3}. Our findings indicate that the chemistry scheme is the prevailing factor influencing Hg concentrations in the Southern Hemisphere, exerting a greater impact than anthropogenic emissions input. These findings demonstrate that intercomparison studies should include region-specific evaluations, recognizing that model accuracy may vary geographically based on different driving factors, rather than focusing only on global model performance. This important effect of anthropogenic emission uncertainties in modeling results leads to a range of RMSE scores in model-observations comparisons that could provide incomplete information about the NH distribution of Hg. Our findings identify high SNR regions, such as Greenland and the eastern U.S., Arctic Russia, and parts of Asia and South America, that can provide reliable observational data to help constrain anthropogenic emission uncertainties and improve model accuracy. The Hg modeling community can improve the reliability of simulations by incorporating more accurate and region-specific anthropogenic Hg emission inventories into models. Trends in atmospheric Hg concentrations, Hg deposition fluxes, changes in national emissions reports provided by Parties, and insights derived from modeling approaches are primary indicators for the effectiveness evaluation under the Minamata Convention (United Nations Environment Programme, 2023). Accurate and consistent emission inventories are essential components in mercury studies, acting as a basis for explaining observed atmospheric trends, verifying reported emissions reductions, and supporting modeling efforts with greater accuracy. The analysis indicates that current uncertainties in emission inventories, particularly in Asia, South America, and Africa, present a significant barrier to reliably assessing progress under the Convention's effectiveness evaluation framework. On a wider level, the results of this study are encouraging collaborative efforts for the refinement of emission inventories and improvement of the accuracy of global Hg models to support policy interventions aimed at mitigating Hg pollution.

5 Acknowledgements

This study was carried out within the GMOS-Train project (www.gmos-train.eu) under the Marie Sklodowska-Curie grant agreement no. 860497 funded by the European Union's Horizon 2020 research and innovation programme. A.F. is funded by the Swiss National Science Foundation (P2EZP2_195424), the US National Science Foundation (no. 1924148), and the Horizon Europe MSCA-PF (101103544). N.E.S. acknowledges support from the U.S. National Science Foundation (1924148). We thank Hélène Angot for the Hg measurement data.

Author contributions

Contributions per Author. Authors are: Charikleia Gournia (C.G.), Prof. Noelle Eckley Selin (N.E.S.), and Dr. Aryeh Feinberg (A.F.). C.G. performed formal analysis, created the visualizations, and wrote the manuscript with contributions from all co-authors. N.E.S. and A.F. supervised the research.

Conflict of interest

None of the authors declare any conflict of interest.

~~Supplementary Information~~

Appendix A

Table A1. Bounding coordinates that were used to calculate the anthropogenic Hg emissions by continent.

Continent	Min Lon	Max Lon	Min Lat	Max Lat
North America	-170.00	-30.00	10.00	83.50
South America	-82.00	-34.00	-56.00	10.00
Europe	-25.00	45.00	38.00	72.00
Africa	-18.00	52.00	-35.00	38.00
Asia	52.00	180.00	-10.00	81.00
Australia	110.00	155.00	-45.00	-10.00

~~Bounding coordinates that were used to calculate the anthropogenic Hg emissions by continent.~~

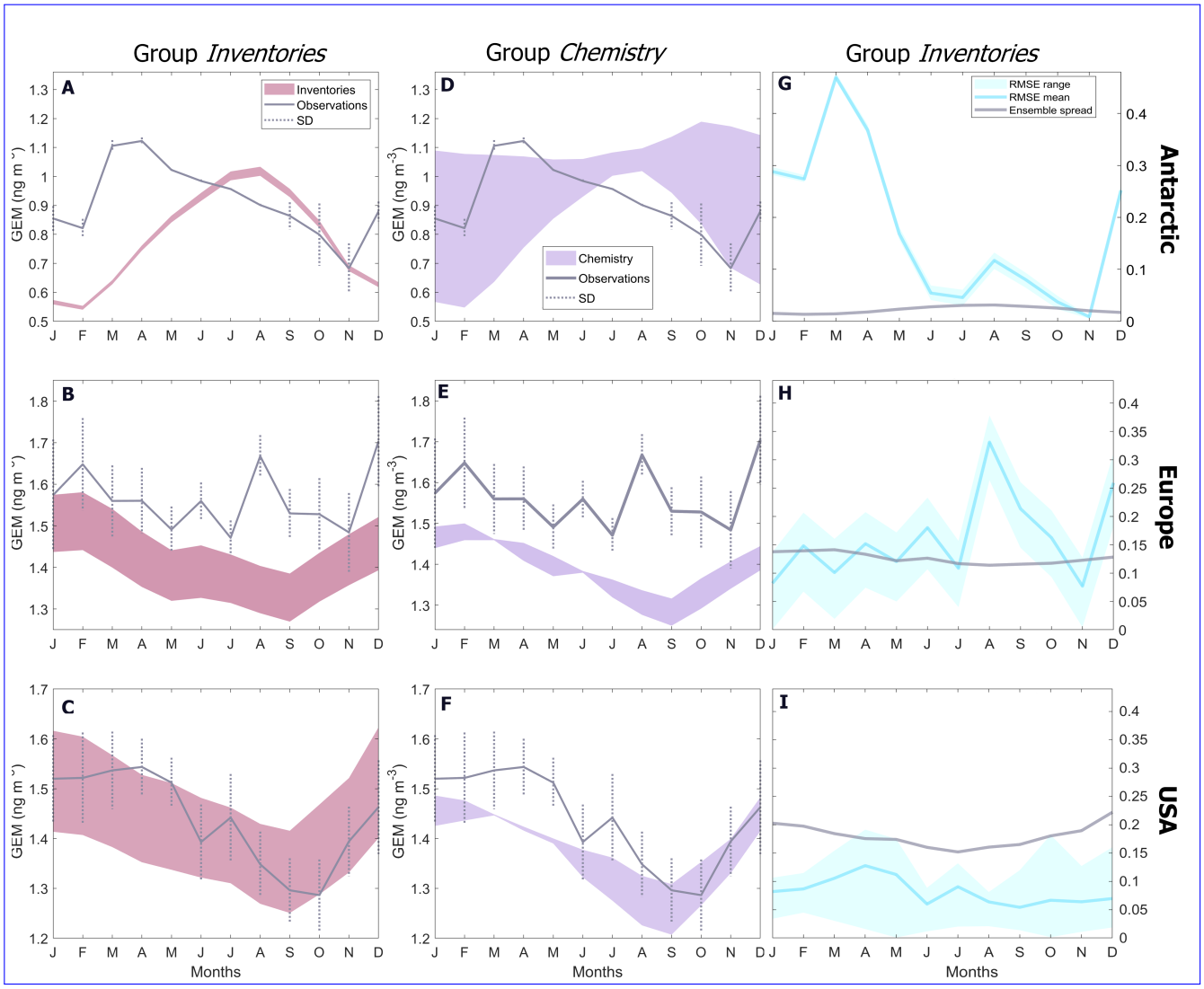

Figure A1. Seasonal variation of ~~TGM~~ GEM (monthly averages and their STD among stations) for stations located in the Antarctic, Europe, and the USA. The range of the simulated ~~TGM~~ GEM is depicted in pink (A-C) and purple (D-F), respectively for the *Inventories* simulations group and *Chemistry* respectively. The third column (G-I) shows the calculated RMSE range and mean ~~,~~ and the group range~~, the daily monthly averaged STD of TGM (model and observations)~~.

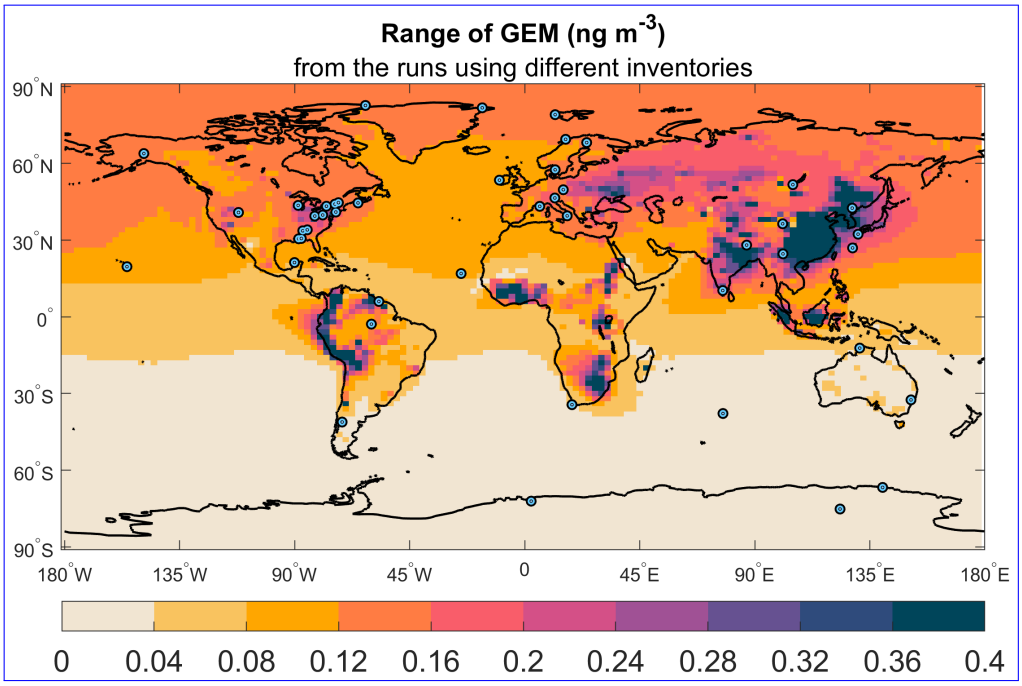

Figure A2. Range of the daily annual mean Hg concentrations for the group of simulations *Inventories*.

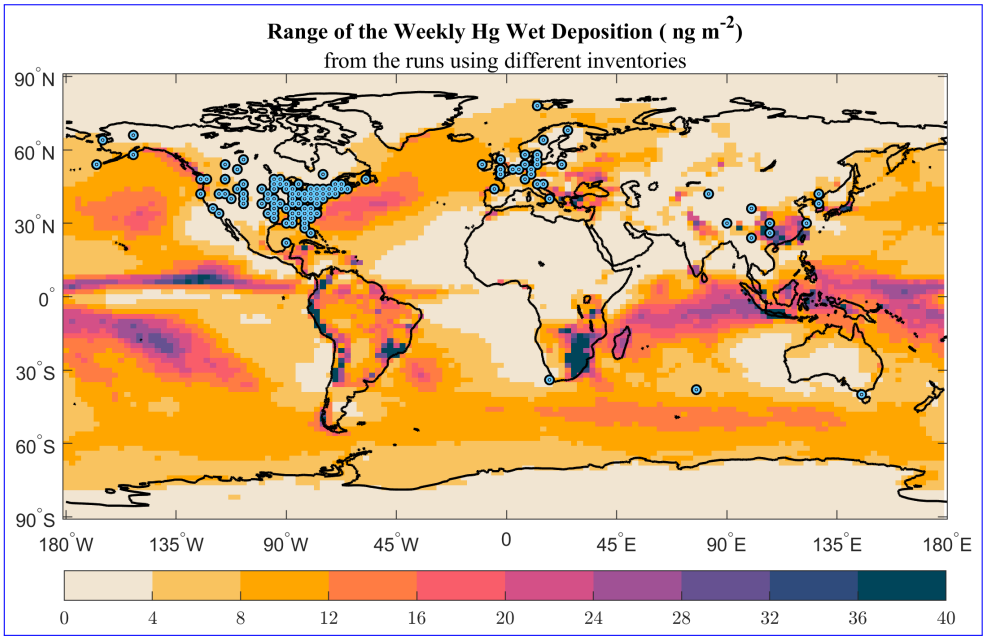

Figure A3. Range of the weekly Hg wet deposition for the group of simulations *Inventories*.

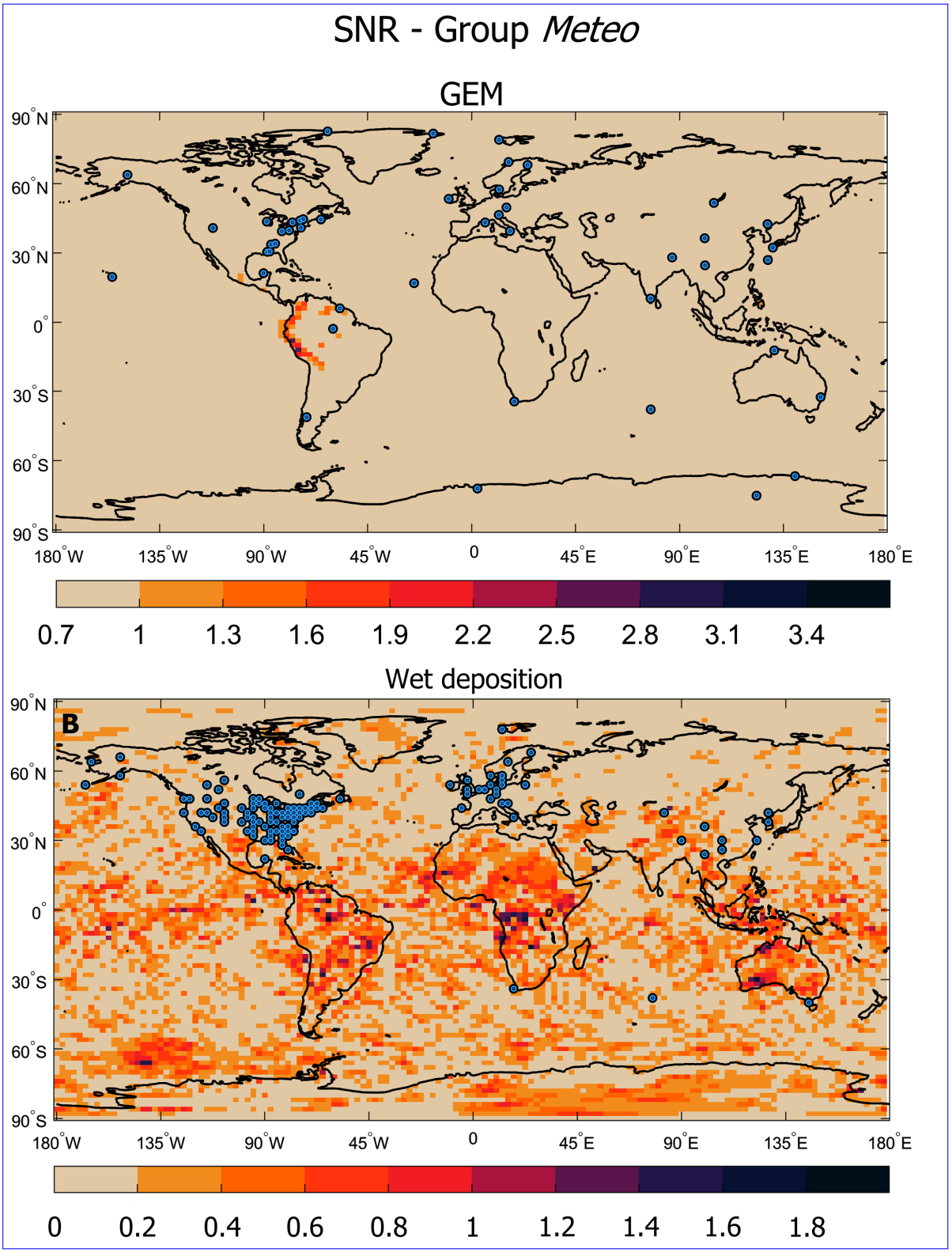

Figure A4. SNR of (A) ~~TGM~~ GEM and (B) wet deposition for the group of simulations *Meteo*.

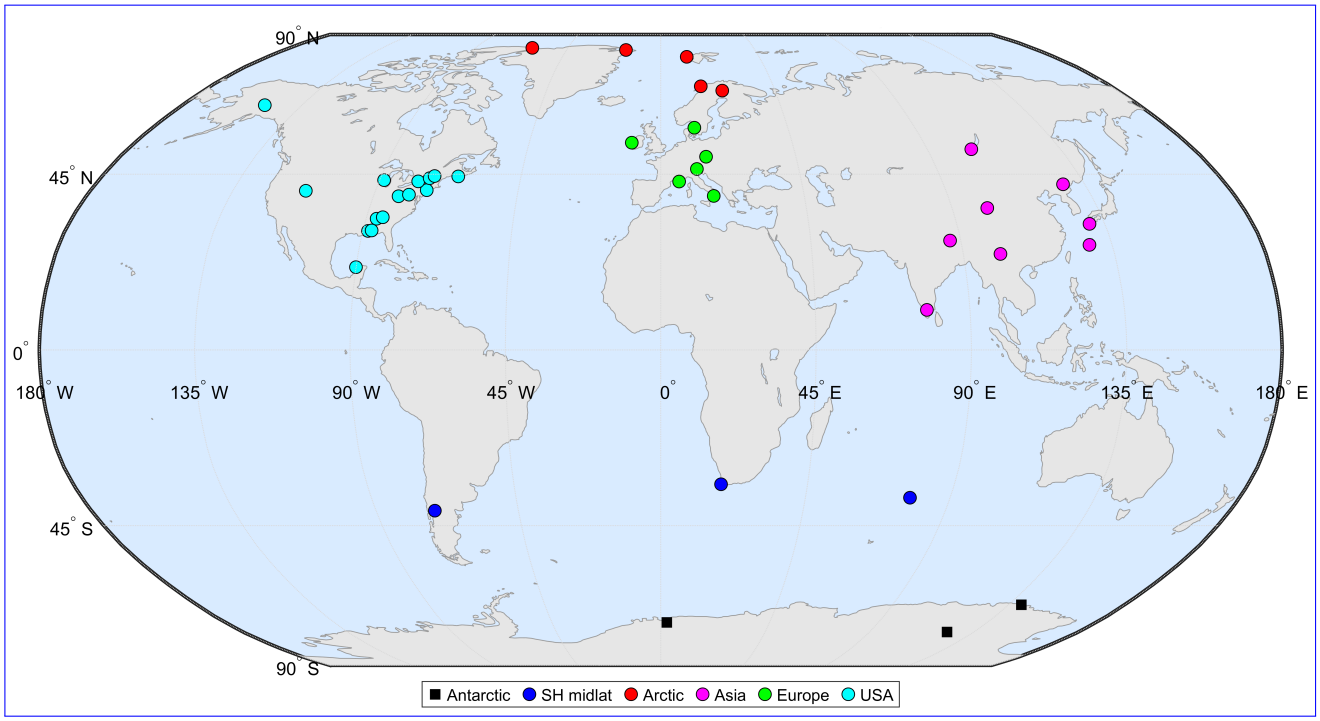

Figure A5. Geographic distribution of categorized GEM monitoring stations used in this study for analysis. Stations are grouped into six regions: Antarctic, Southern Hemisphere midlatitudes, Arctic, Asia, Europe, and USA.

References

Acosta Navarro, J. C. and Toreti, A.: Exploiting the signal to noise ratio in multi-system predictions of summertime precipitation and maximum temperatures in Europe, EGUsphere, 2023, 1–14, https://doi.org/10.5194/egusphere-2023-194, 2023.

Agarwalla, H., Senapati, R. N., and Das, T. B.: Mercury emissions and partitioning from Indian coal-fired power plants, Journal of Environmental Sciences, 100, 28–33, https://doi.org/https://doi.org/10.1016/j.jes.2020.06.035, 2021.

Ahmed, S., Thomas, J. L., Angot, H., Dommergue, A., Archer, S. D., Bariteau, L., Beck, I., Benavent, N., Blechschmidt, A.-M., Blomquist, B., Boyer, M., Christensen, J. H., Dahlke, S., Dastoor, A., Helmig, D., Howard, D., Jacobi, H.-W., Jokinen, T., Lapere, R., Laurila, T., Quéléver, L. L. J., Richter, A., Ryjkov, A., Mahajan, A. S., Marelle, L., Pfaffhuber, K. A., Posman, K., Rinke, A., Saiz-Lopez, A., Schmale, J., Skov, H., Steffen, A., Stupple, G., Stutz, J., Travnikov, O., and Zilker, B.: Modelling the coupled mercury-halogen-ozone cycle in the central Arctic during spring, Elementa: Science of the Anthropocene, 11, 00 129, https://doi.org/10.1525/elementa.2022.00129, 2023.

AMAP/UNEP: Technical Background Report for the Global Mercury Assessment 2013, Arctic Monitoringand Assessment Programme, Oslo, Norway/UNEP ChemicalsBranch, Geneva, Switzerland. vi + 263 pp, 2013.

AMAP/UNEP: Technical Background Report for the Global Mercury Assessment 2018, Arctic Monitoring and Assessment Programme, Oslo, Norway / United Nations Environment Programme, Chemicals and Health Branch, Geneva, Switzerland. viii + 426 pp including E-Annexes, 2019.

Angot, H., Barret, M., Magand, O., Ramonet, M., and Dommergue, A.: A 2-year record of atmospheric mercury species at a background Southern Hemisphere station on Amsterdam Island, Atmospheric Chemistry and Physics, 14, 11 461–11 473, https://doi.org/10.5194/acp-14-11461-2014, 2014.

Angot, H., Dastoor, A., De Simone, F., Gårdfeldt, K., Gencarelli, C. N., Hedgecock, I. M., Langer, S., Magand, O., Mastromonaco, M. N., Nordstrøm, C., Pfaffhuber, K. A., Pirrone, N., Ryjkov, A., Selin, N. E., Skov, H., Song, S., Sprovieri, F., Steffen, A., Toyota, K., Travnikov, O., Yang, X., and Dommergue, A.: Chemical cycling and deposition of atmospheric mercury in polar regions: review of recent measurements and comparison with models, Atmospheric Chemistry and Physics, 16, 10 735–10 763, https://doi.org/10.5194/acp-16-10735-2016, 2016a.

Angot, H., Dion, I., Vogel, N., Legrand, M., Magand, O., and Dommergue, A.: Multi-year record of atmospheric mercury at Dumont d'Urville, East Antarctic coast: continental outflow and oceanic influences, Atmospheric Chemistry and Physics, 16, 8265–8279, https://doi.org/10.5194/acp-16-8265-2016, 2016b.

Angot, H., Magand, O., Helmig, D., Ricaud, P., Quennehen, B., Gallée, H., Del Guasta, M., Sprovieri, F., Pirrone, N., Savarino, J., and Dommergue, A.: New insights into the atmospheric mercury cycling in central Antarctica and implications on a continental scale, Atmospheric Chemistry and Physics, 16, 8249–8264, https://doi.org/10.5194/acp-16-8249-2016, 2016c.

Araujo, B. F., Osterwalder, S., Szponar, N., Lee, D., Petrova, M. V., Pernov, J. B., Ahmed, S., Heimbürger-Boavida, L.-E., Laffont, L., Teisserenc, R., Tananaev, N., Nordstrom, C., Magand, O., Stupple, G., Skov, H., Steffen, A., Bergquist, B., Pfaffhuber, K. A., Thomas, J. L., Scheper, S., Petäjä, T., Dommergue, A., and Sonke, J. E.: Mercury isotope evidence for Arctic summertime re-emission of mercury from the cryosphere, Nature Communications, 13, 4956, https://doi.org/10.1038/s41467-022-32440-8, 2022.

Ariya, P. A., Dastroor, A. P., Amyot, M., Schroeder, W. H., Barrie, L., Anlauf, K., Raofie, F., Ryzhkov, A., Davignon, D., Lalonde, J., and Steffen, A.: The Arctic: a sink for mercury, Tellus B: Chemical and Physical Meteorology, 56, 397–403, https://doi.org/10.3402/tellusb.v56i5.16458, 2004.

Ariya, P. A., Amyot, M., Dastoor, A., Deeds, D., Feinberg, A., Kos, G., Poulain, A., Ryjkov, A., Semeniuk, K., Subir, M., and Toyota, K.: Mercury Physicochemical and Biogeochemical Transformation in the Atmosphere and at Atmospheric Interfaces: A Review and Future Directions, Chem. Rev., 115, 3760–3802, https://doi.org/10.1021/cr500667e, 2015.

Artisanal Gold Council: Global Database on Mercury Emissions from Artisanal and Small Scale Mining (ASGM), www.mercurywatch.org, 2010.

Bich Thao, P. T., Pimonsree, S., Suppoung, K., Bonnet, S., Junpen, A., and Garivait, S.: Development of an anthropogenic atmospheric mercury emissions inventory in Thailand in 2018, Atmospheric Pollution Research, 12, 101 170, https://doi.org/https://doi.org/10.1016/j.apr.2021.101170, 2021.

Bieser, J., Slemr, F., Ambrose, J., Brenninkmeijer, C., Brooks, S., Dastoor, A., DeSimone, F., Ebinghaus, R., Gencarelli, C. N., Geyer, B., Gratz, L. E., Hedgecock, I. M., Jaffe, D., Kelley, P., Lin, C.-J., Jaegle, L., Matthias, V., Ryjkov, A., Selin, N. E., Song, S., Travnikov, O., Weigelt, A., Luke, W., Ren, X., Zahn, A., Yang, X., Zhu, Y., and Pirrone, N.: Multi-model study of mercury dispersion in the atmosphere: vertical and interhemispheric distribution of mercury species, Atmospheric Chemistry and Physics, 17, 6925–6955, https://doi.org/10.5194/acp-17-6925-2017, 2017.

Bieser, J., Angot, H., Slemr, F., and Martin, L.: Atmospheric mercury in the Southern Hemisphere – Part 2: Source apportionment analysis at Cape Point station, South Africa, Atmospheric Chemistry and Physics, 20, 10 427–10 439, https://doi.org/10.5194/acp-20-10427-2020, 2020.

Bruno, D. E., De Simone, F., Cinnirella, S., Hedgecock, I. M., D'Amore, F., and Pirrone, N.: Reducing Mercury Emission Uncertainty from Artisanal and Small-Scale Gold Mining Using Bootstrap Confidence Intervals: An Assessment of Emission Reduction Scenarios, Atmosphere, 14, https://doi.org/10.3390/atmos14010062, 2023.

Bullock Jr., O. R., Atkinson, D., Braverman, T., Civerolo, K., Dastoor, A., Davignon, D., Ku, J.-Y., Lohman, K., Myers, T. C., Park, R. J., Seigneur, C., Selin, N. E., Sistla, G., and Vijayaraghavan, K.: An analysis of simulated wet deposition of mercury from the North American Mercury Model Intercomparison Study, Journal of Geophysical Research: Atmospheres, 114, https://doi.org/https://doi.org/10.1029/2008JD011224, 2009.

Castro, P., Kellö, V., Cernušák, I., and Dibble, T.: Together, not separately, OH and O3 oxidize Hg(0) to Hg(II) in the atmosphere, ChemRxiv. Cambridge: Cambridge Open Engage, 2022.

Cement Sustainability Initiative: Getting the numbers right (GNR) database, Cement Sustainability Initiative, http://www.wbcsdcement.org/GNR-2012/index.html, 2016.

Cinnirella, S. and Pirrone, N.: An uncertainty estimate of global mercury emissions using the Monte Carlo technique, E3S Web of Conferences, 1, 07 006, https://doi.org/10.1051/e3sconf/20130107006, 2013.

Corbitt, E. S., Jacob, D. J., Holmes, C. D., Streets, D. G., and Sunderland, E. M.: Global Source–Receptor Relationships for Mercury Deposition Under Present-Day and 2050 Emissions Scenarios, Environmental Science & Technology, 45, 10 477–10 484, https://doi.org/10.1021/es202496y, pMID: 22050654, 2011.

Cui, Y., Wu, Q., Wang, S., Liu, K., Li, S., Shi, Z., Ouyang, D., Li, Z., Chen, Q., Lü, C., Xie, F., Tang, Y., Wang, Y., and Hao, J.: Integrating point sources to map anthropogenic atmospheric mercury emissions in China, 1978–2021, Earth System Science Data, 17, 3315–3328, https://doi.org/10.5194/essd-17-3315-2025, 2025.

Dastoor, A., Ryzhkov, A., Durnford, D., Lehnherr, I., Steffen, A., and Morrison, H.: Atmospheric mercury in the Canadian Arctic. Part II: Insight from modeling, Science of The Total Environment, 509-510, 16–27, https://doi.org/https://doi.org/10.1016/j.scitotenv.2014.10.112, special Issue: Mercury in Canada's North, 2015.

Dastoor, A., Angot, H., Bieser, J., Christensen, J. H., Douglas, T. A., Heimbürger-Boavida, L.-E., Jiskra, M., Mason, R. P., McLagan, D. S., Obrist, D., Outridge, P. M., Petrova, M. V., Ryjkov, A., St. Pierre, K. A., Schartup, A. T., Soerensen, A. L., Toyota, K., Travnikov, O., Wilson, S. J., and Zdanowicz, C.: Arctic mercury cycling, Nature Reviews Earth Environment, 3, 270–286, https://doi.org/10.1038/s43017-022-00269-w, 2022a.

Dastoor, A., Wilson, S. J., Travnikov, O., Ryjkov, A., Angot, H., Christensen, J. H., Steenhuisen, F., and Muntean, M.: Arctic atmospheric mercury: Sources and changes, Science of The Total Environment, 839, 156 213, https://doi.org/https://doi.org/10.1016/j.scitotenv.2022.156213, 2022b.

Dastoor, A., Angot, H., Bieser, J., Brocza, F., Edwards, B., Feinberg, A., Feng, X., Geyman, B., Gournia, C., He, Y., Hedgecock, I. M., Ilyin, I., Keating, T., Kirk, J., Lin, C.-J., Lehnherr, I., Mason, R., McLagan, D., Muntean, M., Rafaj, P., Roy, E. M., Ryjkov, A., Selin, N. E., De Simone, F., Soerensen, A. L., Steenhuisen, F., Travnikov, O., Wang, S., Wang, X., Wilson, S., Wu, R., Wu, Q., Zhang, Y., Zhou, J., Zhu, W., and Zolkos, S.: The Multi-Compartment Hg Modeling and Analysis Project (MCHgMAP): Mercury modeling to support international environmental policy, Geoscientific Model Development Discussions, 2024, 1–171, https://doi.org/10.5194/gmd-2024-65, 2025.

De Simone, F., Hedgecock, I. M., Carbone, F., Cinnirella, S., Sprovieri, F., and Pirrone, N.: Estimating Uncertainty in Global Mercury Emission Source and Deposition Receptor Relationships, Atmosphere, 8, https://doi.org/10.3390/atmos8120236, 2017.

Dlamini, T.: Assessing the role of top-down techniques for improving regional estimates of artisanal and small-scale gold mining mercury emissions., Massachusetts Institute of Technology, https://dspace.mit.edu/handle/1721.1/147481, 2022.

Doi, T., Nonaka, M., and Behera, S.: Can signal-to-noise ratio indicate prediction skill? Based on skill assessment of 1-month lead prediction of monthly temperature anomaly over Japan, Frontiers in Climate, 4, https://doi.org/10.3389/fclim.2022.887782, 2022.

Dommergue, A., Sprovieri, F., Pirrone, N., Ebinghaus, R., Brooks, S., Courteaud, J., and Ferrari, C. P.: Overview of mercury measurements in the Antarctic troposphere, Atmospheric Chemistry and Physics, 10, 3309–3319, https://doi.org/10.5194/acp-10-3309-2010, 2010.

Dommergue, A., Ferrari, C. P., Magand, O., Barret, M., Gratz, L. E., Pirrone, N., and Sprovieri, F.: Monitoring of gaseous elemental mercury in central Antarctica at Dome Concordia, E3S Web of Conferences, 1, 17 003, https://doi.org/10.1051/e3sconf/20130117003, 2013.

Driscoll, C. T., Mason, R. P., Chan, H. M., Jacob, D. J., and Pirrone, N.: Mercury as a Global Pollutant: Sources, Pathways, and Effects, Environmental Science & Technology, 47, 4967–4983, https://doi.org/10.1021/es305071v, pMID: 23590191, 2013.

Durnford, D. and Dastoor, A.: The behavior of mercury in the cryosphere: A review of what we know from observations, Journal of Geophysical Research: Atmospheres, 116, https://doi.org/https://doi.org/10.1029/2010JD014809, 2011.

Durnford, D., Dastoor, A., Figueras-Nieto, D., and Ryjkov, A.: Long range transport of mercury to the Arctic and across Canada, Atmospheric Chemistry and Physics, 10, 6063–6086, https://doi.org/10.5194/acp-10-6063-2010, 2010.

EMEP/EEA: European Monitoring and Evaluation Programme/European Environment Agency, Air pollutant emission inventory guidebook. Technical report No 12/2013., http://www.eea.europa.eu/publications/emep-eea-guidebook2013, 2013.

Falkena, S. K., de Wiljes, J., Weisheimer, A., and Shepherd, T. G.: Detection of interannual ensemble forecast signals over the North Atlantic and Europe using atmospheric circulation regimes, Quarterly Journal of the Royal Meteorological Society, 148, 434–453, https://doi.org/https://doi.org/10.1002/qj.4213, 2022.

FAO: Food and agriculture organization of the United Nations., http://www.fao.org, 2015.

Feinberg, A., Dlamini, T., Jiskra, M., Shah, V., and Selin, N. E.: Evaluating atmospheric mercury (Hg) uptake by vegetation in a chemistry-transport model, Environ. Sci.: Processes Impacts, 24, 1303–1318, https://doi.org/10.1039/D2EM00032F, 2022.

Feinberg, A., Jiskra, M., Borrelli, P., Biswakarma, J., and Selin, N. E.: Deforestation as an Anthropogenic Driver of Mercury Pollution, Environmental Science & Technology, 58, 3246–3257, https://doi.org/10.1021/acs.est.3c07851, pMID: 38328901, 2024a.

Feinberg, A., Selin, N. E., Braban, C. F., Chang, K.-L., Custódio, D., Jaffe, D. A., Kyllönen, K., Landis, M. S., Leeson, S. R., Luke, W., Molepo, K. M., Murovec, M., Mastromonaco, M. G. N., Pfaffhuber, K. A., Rüdiger, J., Sheu, G.-R., and Louis, V. L. S.: Unexpected anthropogenic emission decreases explain recent atmospheric mercury concentration declines, Proceedings of the National Academy of Sciences, 121, e2401950 121, https://doi.org/10.1073/pnas.2401950121, 2024b.

Fisher, J. A., Jacob, D. J., Soerensen, A. L., Amos, H. M., Steffen, A., and Sunderland, E. M.: Riverine source of Arctic Ocean mercury inferred from atmospheric observations, Nature Geoscience, 5, 499–504, https://doi.org/10.1038/ngeo1478, 2012.

Fu, X., Yang, X., Lang, X., Zhou, J., Zhang, H., Yu, B., Yan, H., Lin, C.-J., and Feng, X.: Atmospheric wet and litterfall mercury deposition at urban and rural sites in China, Atmospheric Chemistry and Physics, 16, 11 547–11 562, https://doi.org/10.5194/acp-16-11547-2016, 2016.

Gabay, M., Raveh-Rubin, S., Peleg, M., Fredj, E., and Tas, E.: Is oxidation of atmospheric mercury controlled by different mechanisms in the polluted continental boundary layer vs. remote marine boundary layer?, Environmental Research Letters, 15, 064 026, https://doi.org/10.1088/1748-9326/ab7b26, 2020.

Guo, J., Liu, L., Zhang, G., Yue, R., Wang, T., Zhang, X., Yang, S., Zhang, Y., Wang, K., Long, H., Feng, Q., and Chen, Y.: Temporal and spatial analysis of anthropogenic mercury and CO2 emissions from municipal solid waste incineration in China: Implications for mercury and climate change mitigation, Environment International, 178, 108 068, https://doi.org/https://doi.org/10.1016/j.envint.2023.108068, 2023.

Gustin, M. S., Bank, M. S., Bishop, K., Bowman, K., Branfireun, B., Chételat, J., Eckley, C. S., Hammerschmidt, C. R., Lamborg, C., Lyman, S., Martínez-Cortizas, A., Sommar, J., Tsui, M. T.-K., and Zhang, T.: Mercury biogeochemical cycling: A synthesis of recent scientific advances., The Science of the total environment, 737, 139 619, 2020.

Gustin, M. S., Dunham-Cheatham, S. M., Huang, J., Lindberg, S., and Lyman, S. N.: Development of an Understanding of Reactive Mercury in Ambient Air: A Review, Atmosphere, 12, https://doi.org/10.3390/atmos12010073, 2021.

Hamilton, R. J. and Hart, M.: Development and verification of the signal to noise ratio for a layer of turbulence in a multi-layer atmosphere., Journal of the Optical Society of America. A, Optics, image science, and vision, 40, 573–582, 2023.

Hasselmann, K.: On the signal-to-noise problem in atmospheric response studies, https://api.semanticscholar.org/CorpusID:164816613, 1979.

Holmes, C. D., Jacob, D. J., Corbitt, E. S., Mao, J., Yang, X., Talbot, R., and Slemr, F.: Global atmospheric model for mercury including oxidation by bromine atoms, Atmospheric Chemistry and Physics, 10, 12 037–12 057, https://doi.org/10.5194/acp-10-12037-2010, 2010.

Horowitz, H. M., Jacob, D. J., Amos, H. M., Streets, D. G., and Sunderland, E. M.: Historical Mercury Releases from Commercial Products: Global Environmental Implications, Environmental Science & Technology, 48, 10 242–10 250, https://doi.org/10.1021/es501337j, pMID: 25127072, 2014.

Horowitz, H. M., Jacob, D. J., Zhang, Y., Dibble, T. S., Slemr, F., Amos, H. M., Schmidt, J. A., Corbitt, E. S., Marais, E. A., and Sunderland, E. M.: A new mechanism for atmospheric mercury redox chemistry: implications for the global mercury budget, Atmospheric Chemistry and Physics, 17, 6353–6371, https://doi.org/10.5194/acp-17-6353-2017, 2017.

Huang, S., Wang, F., Yuan, T., Song, Z., Wu, P., and Zhang, Y.: Modeling the Mercury Cycle in the Sea Ice Environment: A Buffer between the Polar Atmosphere and Ocean, Environmental Science & Technology, 57, 14 589–14 601, https://doi.org/10.1021/acs.est.3c05080, pMID: 37585923, 2023.

Huang, S., Yuan, T., Song, Z., et al.: Oceanic evasion fuels Arctic summertime rebound of atmospheric mercury and drives transport to Arctic terrestrial ecosystems, Nature Communications, 16, 903, https://doi.org/10.1038/s41467-025-56300-3, 2025.

Huang, Y., Deng, M., Li, T., Japenga, J., Chen, Q., Yang, X., and He, Z.: Anthropogenic mercury emissions from 1980 to 2012 in China, Environmental Pollution, 226, 230–239, https://doi.org/https://doi.org/10.1016/j.envpol.2017.03.059, 2017.

IEA: International Energy agency, http://www.iea.org.

Joy, A. and Qureshi, A.: Reducing mercury emissions from coal-fired power plants in India: Possibilities and challenges, Ambio, 52, 242–252, https://doi.org/10.1007/s13280-022-01773-5, 2023.

Kogut, K., Górecki, J., and Burmistrz, P.: Opportunities for reducing mercury emissions in the cement industry, Journal of Cleaner Production, 293, 126 053, https://doi.org/https://doi.org/10.1016/j.jclepro.2021.126053, 2021.

Kosai, S., Nakajima, K., and Yamasue, E.: Mercury mitigation and unintended consequences in artisanal and small-scale gold mining, Resources, Conservation and Recycling, 188, 106 708, https://doi.org/https://doi.org/10.1016/j.resconrec.2022.106708, 2023.

Kwon, S. Y. and Selin, N. E.: Uncertainties in Atmospheric Mercury Modeling for Policy Evaluation, Current Pollution Reports, 2, 103–114, https://doi.org/10.1007/s40726-016-0030-8, 2016.

Lindberg, S., Bullock, R., Ebinghaus, R., Engstrom, D., Feng, X., Fitzgerald, W., Pirrone, N., Prestbo, E., and Seigneur, C.: A Synthesis of Progress and Uncertainties in Attributing the Sources of Mercury in Deposition, AMBIO: A Journal of the Human Environment, 36, 19 – 33, https://doi.org/10.1579/0044-7447(2007)36[19:ASOPAU]2.0.CO;2, 2007.

Liu, H., Jacob, D. J., Bey, I., and Yantosca, R. M.: Constraints from 210Pb and 7Be on wet deposition and transport in a global three-dimensional chemical tracer model driven by assimilated meteorological fields, Journal of Geophysical Research: Atmospheres, 106, 12 109–12 128, https://doi.org/https://doi.org/10.1029/2000JD900839, 2001.

Liu, K., Wu, Q., Wang, L., Wang, S., Liu, T., Ding, D., Tang, Y., Li, G., Tian, H., Duan, L., Wang, X., Fu, X., Feng, X., and Hao, J.: Measure-Specific Effectiveness of Air Pollution Control on China's Atmospheric Mercury Concentration and Deposition during 2013–2017, Environmental Science & Technology, 53, 8938–8946, https://doi.org/10.1021/acs.est.9b02428, pMID: 31242727, 2019.

MacFarlane, S., Fisher, J. A., Horowitz, H. M., and Shah, V.: Two decades of changing anthropogenic mercury emissions in Australia: inventory development, trends, and atmospheric implications, Environmental Science: Processes and Impacts, 24, 1474–1493, https://doi.org/10.1039/D2EM00019A, 2022.

Mao, H., Cheng, I., and Zhang, L.: Current understanding of the driving mechanisms for spatiotemporal variations of atmospheric speciated mercury: a review, Atmospheric Chemistry and Physics, 16, 12 897–12 924, https://doi.org/10.5194/acp-16-12897-2016, 2016.

Matthias, V., Aulinger, A., Bieser, J., and Quante, M.: Regional modeling of atmospheric mercury: impact of meteorological variables, https://api.semanticscholar.org/CorpusID:98545374, 2013.

Mulvaney, K. M., Selin, N. E., Giang, A., Muntean, M., Li, C.-T., Zhang, D., Angot, H., Thackray, C. P., and Karplus, V. J.: Mercury Benefits of Climate Policy in China: Addressing the Paris Agreement and the Minamata Convention Simultaneously., Environmental science technology, 54, 1326–1335, 2020.

Muntean, M., Janssens-Maenhout, G., Song, S., Selin, N. E., Olivier, J. G., Guizzardi, D., Maas, R., and Dentener, F.: Trend analysis from 1970 to 2008 and model evaluation of EDGARv4 global gridded anthropogenic mercury emissions, Science of The Total Environment, 494-495, 337–350, https://doi.org/https://doi.org/10.1016/j.scitotenv.2014.06.014, 2014.

Muntean, M., Janssens-Maenhout, G., Song, S., Giang, A., Selin, N. E., Zhong, H., Zhao, Y., Olivier, J. G., Guizzardi, D., Crippa, M., Schaaf, E., and Dentener, F.: Evaluating EDGARv4.tox2 speciated mercury emissions ex-post scenarios and their impacts on modelled global and regional wet deposition patterns, Atmospheric Environment, 184, 56–68, https://doi.org/https://doi.org/10.1016/j.atmosenv.2018.04.017, 2018.

Muntean, M., Crippa, M., Guizzardi, D., Pagani, F., Becker, W., Banja, M., Schaaf, E., and Simonati, A.: EDGAR v8.1 Global Mercury Emissions, https://doi.org/10.2905/83b507d7-5218-4dc5-95f9-0ec36f073204, dataset, 2024.

Pacyna, J. M., Travnikov, O., De Simone, F., Hedgecock, I. M., Sundseth, K., Pacyna, E. G., Steenhuisen, F., Pirrone, N., Munthe, J., and Kindbom, K.: Current and future levels of mercury atmospheric pollution on a global scale, Atmospheric Chemistry and Physics, 16, 12 495–12 511, https://doi.org/10.5194/acp-16-12495-2016, 2016.

Pfaffhuber, K. A., Berg, T., Hirdman, D., and Stohl, A.: Atmospheric mercury observations from Antarctica: seasonal variation and source and sink region calculations, Atmospheric Chemistry and Physics, 12, 3241–3251, https://doi.org/10.5194/acp-12-3241-2012, 2012.

Qiu, X., Liu, M., Zhang, Y., et al.: Declines in anthropogenic mercury emissions in the Global North and China offset by the Global South, Nature Communications, 16, 1179, https://doi.org/10.1038/s41467-025-56274-2, 2025.

Qureshi, A., MacLeod, M., and Hungerbühler, K.: Quantifying uncertainties in the global mass balance of mercury, Global Biogeochemical Cycles, 25, https://doi.org/https://doi.org/10.1029/2011GB004068, 2011.

Ryaboshapko, A., Bullock, O. R., Christensen, J., Cohen, M., Dastoor, A., Ilyin, I., Petersen, G., Syrakov, D., Artz, R. S., Davignon, D., Draxler, R. R., and Munthe, J.: Intercomparison study of atmospheric mercury models: 1. Comparison of models with short-term measurements, Science of The Total Environment, 376, 228–240, https://doi.org/https://doi.org/10.1016/j.scitotenv.2007.01.072, 2007.

Saiz-Lopez, A., Travnikov, O., Sonke, J. E., Thackray, C. P., Jacob, D. J., Carmona-García, J., Francés-Monerris, A., Roca-Sanjuán, D., Acuña, A. U., Dávalos, J. Z., Cuevas, C. A., Jiskra, M., Wang, F., Bieser, J., Plane, J. M. C., and Francisco, J. S.: Photochemistry of oxidized Hg(I) and Hg(II) species suggests missing mercury oxidation in the troposphere, Proceedings of the National Academy of Sciences of the United States of America, 117, 30 949–30 956, https://doi.org/10.1073/pnas.1922486117, 2020.

Saiz-Lopez, A., Mahajan, A. S., Abbatt, J. P. D., et al.: The influence of short-lived halogens on atmospheric chemistry and climate, Nature, 648, 289–299, https://doi.org/10.1038/s41586-025-09753-x, 2025.

Schmidt, J. A., Jacob, D. J., Horowitz, H. M., Hu, L., Sherwen, T., Evans, M. J., Liang, Q., Suleiman, R. M., Oram, D. E., Le Breton, M., Percival, C. J., Wang, S., Dix, B., and Volkamer, R.: Modeling the observed tropospheric BrO background: Importance of multiphase chemistry and implications for ozone, OH, and mercury, Journal of Geophysical Research: Atmospheres, 121, 11,819–11,835, https://doi.org/https://doi.org/10.1002/2015JD024229, 2016.

Schneider, L., Fisher, J. A., Diéguez, M. C., Fostier, A.-H., Guimaraes, J. R. D., Leaner, J. J., and Mason, R.: A synthesis of mercury research in the Southern Hemisphere, part 1: Natural processes, Ambio, 52, 897–917, https://doi.org/10.1007/s13280-023-01832-5, 2023.

Selin, N. E., Jacob, D. J., Yantosca, R. M., Strode, S., Jaeglé, L., and Sunderland, E. M.: Global 3-D land-ocean-atmosphere model for mercury: Present-day versus preindustrial cycles and anthropogenic enrichment factors for deposition, Global Biogeochemical Cycles, 22, https://doi.org/https://doi.org/10.1029/2007GB003040, 2008.

Shah, V., Jacob, D. J., Thackray, C. P., Wang, X., Sunderland, E. M., Dibble, T. S., Saiz-Lopez, A., Černušák, I., Kellö, V., Castro, P. J., Wu, R., and Wang, C.: Improved Mechanistic Model of the Atmospheric Redox Chemistry of Mercury, Environ. Sci. Technol., https://doi.org/10.1021/acs.est.1c03160, 2021.

Simone, F. D., Gencarelli, C. N., Hedgecock, I. M., and Pirrone, N.: A Modeling Comparison of Mercury Deposition from Current Anthropogenic Mercury Emission Inventories, Environ. Sci. Technol., 50, 5154–5162, https://doi.org/10.1021/acs.est.6b00691, 2016.

Skov, H., Christensen, J. H., Goodsite, M. E., Heidam, N. Z., Jensen, B., Wåhlin, P., and Geernaert, G.: Fate of Elemental Mercury in the Arctic during Atmospheric Mercury Depletion Episodes and the Load of Atmospheric Mercury to the Arctic, Environmental Science & Technology, 38, 2373–2382, https://doi.org/10.1021/es030080h, pMID: 15116843, 2004.

Skov, H., Hjorth, J., Nordstrøm, C., Jensen, B., Christoffersen, C., Bech Poulsen, M., Baldtzer Liisberg, J., Beddows, D., Dall'Osto, M., and Christensen, J. H.: Variability in gaseous elemental mercury at Villum Research Station, Station Nord, in North Greenland from 1999 to 2017, Atmospheric Chemistry and Physics, 20, 13 253–13 265, https://doi.org/10.5194/acp-20-13253-2020, 2020.

Slemr, F., Martin, L., Labuschagne, C., Mkololo, T., Angot, H., Magand, O., Dommergue, A., Garat, P., Ramonet, M., and Bieser, J.: Atmospheric mercury in the Southern Hemisphere – Part 1: Trend and inter-annual variations in atmospheric mercury at Cape Point, South Africa, in 2007–2017, and on Amsterdam Island in 2012–2017, Atmospheric Chemistry and Physics, 20, 7683–7692, https://doi.org/10.5194/acp-20-7683-2020, 2020.

Song, S., Selin, N. E., Soerensen, A. L., Angot, H., Artz, R., Brooks, S., Brunke, E.-G., Conley, G., Dommergue, A., Ebinghaus, R., Holsen, T. M., Jaffe, D. A., Kang, S., Kelley, P., Luke, W. T., Magand, O., Marumoto, K., Pfaffhuber, K. A., Ren, X., Sheu, G.-R., Slemr, F., Warneke, T., Weigelt, A., Weiss-Penzias, P., Wip, D. C., and Zhang, Q.: Top-down constraints on atmospheric mercury emissions and implications for global biogeochemical cycling, Atmospheric Chemistry and Physics, 15, 7103–7125, https://doi.org/10.5194/acp-15-7103-2015, 2015.

Sprovieri, F., Pirrone, N., Hedgecock, I. M., Landis, M. S., and Stevens, R. K.: Intensive atmospheric mercury measurements at Terra Nova Bay in Antarctica during November and December 2000, Journal of Geophysical Research: Atmospheres, 107, ACH 20–1–ACH 20–8, https://doi.org/https://doi.org/10.1029/2002JD002057, 2002.

Sprovieri, F., Pirrone, N., Bencardino, M., D'Amore, F., Angot, H., Barbante, C., Brunke, E.-G., Arcega-Cabrera, F., Cairns, W., Comero, S., Diéguez, M. D. C., Dommergue, A., Ebinghaus, R., Feng, X. B., Fu, X., Garcia, P. E., Gawlik, B. M., Hageström, U., Hansson, K., Horvat, M., Kotnik, J., Labuschagne, C., Magand, O., Martin, L., Mashyanov, N., Mkololo, T., Munthe, J., Obolkin, V., Ramirez Islas, M., Sena, F., Somerset, V., Spandow, P., Vardè, M., Walters, C., Wängberg, I., Weigelt, A., Yang, X., and Zhang, H.: Five-year records of mercury wet deposition flux at GMOS sites in the Northern and Southern hemispheres, Atmospheric Chemistry and Physics, 17, 2689–2708, https://doi.org/10.5194/acp-17-2689-2017, 2017.

Steenhuisen, F. and Wilson, S.: Development and application of an updated geospatial distribution model for gridding 2015 global mercury emissions, Atmospheric Environment, 211, 138–150, https://doi.org/https://doi.org/10.1016/j.atmosenv.2019.05.003, 2019.

Steenhuisen, F. and Wilson, S.: Geospatially Distributed (Gridded) Global Mercury Emissions to Air from Anthropogenic Sources in 2015, https://doi.org/10.34894/SZ2KOI, 2022.

Steffen, A., Douglas, T., Amyot, M., Ariya, P., Aspmo, K., Berg, T., Bottenheim, J., Brooks, S., Cobbett, F., Dastoor, A., Dommergue, A., Ebinghaus, R., Ferrari, C., Gardfeldt, K., Goodsite, M. E., Lean, D., Poulain, A. J., Scherz, C., Skov, H., Sommar, J., and Temme, C.: A synthesis of atmospheric mercury depletion event chemistry in the atmosphere and snow, Atmospheric Chemistry and Physics, 8, 1482, https://hal.archives-ouvertes.fr/hal-00328572, 2008.

Streets, D. G., Zhang, Q., and Wu, Y.: Projections of Global Mercury Emissions in 2050, Environmental Science & Technology, 43, 2983–2988, https://doi.org/10.1021/es802474j, pMID: 19475981, 2009.

Streets, D. G., Horowitz, H. M., Lu, Z., Levin, L., Thackray, C. P., and Sunderland, E. M.: Global and regional trends in mercury emissions and concentrations, 2010-2015, Atmospheric Environment, 201, 417–427, https://doi.org/10.1016/j.atmosenv.2018.12.031, 2019.

Subir, M., Ariya, P. A., and Dastoor, A. P.: A review of the sources of uncertainties in atmospheric mercury modeling II. Mercury surface and heterogeneous chemistry – A missing link, Atmospheric Environment, 46, 1–10, https://doi.org/https://doi.org/10.1016/j.atmosenv.2011.07.047, 2012.

Temme, C., Einax, J. W., Ebinghaus, R., and Schroeder, W. H.: Measurements of Atmospheric Mercury Species at a Coastal Site in the Antarctic and over the South Atlantic Ocean during Polar Summer, Environ. Sci. Technol., 37, 22–31, https://doi.org/10.1021/es025884w, 2003.

Travnikov, O., Angot, H., Artaxo, P., Bencardino, M., Bieser, J., D'Amore, F., Dastoor, A., De Simone, F., Diéguez, M. D. C., Dommergue, A., Ebinghaus, R., Feng, X. B., Gencarelli, C. N., Hedgecock, I. M., Magand, O., Martin, L., Matthias, V., Mashyanov, N., Pirrone, N., Ramachandran, R., Read, K. A., Ryjkov, A., Selin, N. E., Sena, F., Song, S., Sprovieri, F., Wip, D., Wängberg, I., and Yang, X.: Multi-model study of mercury dispersion in the atmosphere: atmospheric processes and model evaluation, Atmospheric Chemistry and Physics, 17, 5271–5295, https://doi.org/10.5194/acp-17-5271-2017, 2017.

UNEP: United Nations Environment Programme: Hemispheric Transport of Air Pollution, Part B: Mercury, https://wedocs.unep.org/20.500.11822/12326, 2010.

UNEP: United Nations Environment Programme Basel Convention Regional Centre For South East Asia, Mercury Emissions for Coal-Fired Power Plants in Indonesia, https://www.unep.org/, 2017a.

UNEP: United Nations Environment Programme: Global Mercury Supply, Trade and Demand, https://www.unep.org/resources/report/global-mercury-supply-trade-and-demand, 2017b.

UNFCCC: United Nations Framework Convention on Climate Change: national reports, http://unfccc.int/national_reports/items/1408.php, 2015.

United Nations Environment Programme: Indicators (Addendum 1 to document COP.5/16), https://minamataconvention.org/sites/default/files/documents/working_document/UNEP-MC-COP.5-16-Add.1-Indicators_English.pdf, accessed: 2025-08-09, 2023.

USGS: United States Geological Survey, Commodity statistics and information, http://minerals.usgs.gov/minerals/pubs/commodity/, 2015.

Wang, F., Saiz-Lopez, A., Mahajan, A. S., Gómez Martín, J. C., Armstrong, D., Lemes, M., Hay, T., and Prados-Roman, C.: Enhanced production of oxidised mercury over the tropical Pacific Ocean: a key missing oxidation pathway, Atmospheric Chemistry and Physics, 14, 1323–1335, https://doi.org/10.5194/acp-14-1323-2014, 2014.

Wang, J., Liu, L., Li, S., Chen, Y., Wang, T., and Zhang, Y.: Mercury emissions and distribution in a waste incineration plant based on the 30B and Ontario Hydro methods, Journal of Cleaner Production, 328, 129 663, https://doi.org/https://doi.org/10.1016/j.jclepro.2021.129663, 2021.

Welvaert, M. and Rosseel, Y.: On the definition of signal-to-noise ratio and contrast-to-noise ratio for FMRI data., PloS one, 8, e77 089, 2013.

Wesely, M. L.: Parameterization of surface resistances to gaseous dry deposition in regional-scale numerical models, Atmospheric Environment, 23, 1293–1304, https://doi.org/10.1016/0004-6981(89)90153-4, 1989.

Wu, Q., Wang, S., Li, G., Liang, S., Lin, C.-J., Wang, Y., Cai, S., Liu, K., and Hao, J.: Temporal Trend and Spatial Distribution of Speciated Atmospheric Mercury Emissions in China During 1978-2014, Environ. Sci. Technol., 50, 13 428–13 435, https://doi.org/10.1021/acs.est.6b04308, 2016.

Wu, W., Lynch, A. H., and Rivers, A.: Estimating the Uncertainty in a Regional Climate Model Related to Initial and Lateral Boundary Conditions, Journal of Climate, 18, 917 – 933, https://doi.org/10.1175/JCLI-3293.1, 2005.

Wu, Y., Streets, D. G., Wang, S. X., and Hao, J. M.: Uncertainties in estimating mercury emissions from coal-fired power plants in China, Atmospheric Chemistry and Physics, 10, 2937–2946, https://doi.org/10.5194/acp-10-2937-2010, 2010.

Xu, J.-H., Fleiter, T., Fan, Y., and Eichhammer, W.: CO2 emissions reduction potential in China's cement industry compared to IEA's Cement Technology Roadmap up to 2050, Applied Energy, 130, 592–602, https://doi.org/https://doi.org/10.1016/j.apenergy.2014.03.004, 2014.

Xu, Z., Chen, L., Zhang, Y., Han, G., Chen, Q., Chu, Z., Zhang, Y., Li, C., Yang, Y., and Wang, X.: Meteorological Drivers of Atmospheric Mercury Seasonality in the Temperate Northern Hemisphere, Geophysical Research Letters, 49, e2022GL100 120, https://doi.org/https://doi.org/10.1029/2022GL100120, e2022GL100120 2022GL100120, 2022.

Yang, M., Wang, S., Zhang, L., Wu, Q., Wang, F., Hui, M., Yang, H., and Hao, J.: Mercury emission and speciation from industrial gold production using roasting process, Journal of Geochemical Exploration, 170, 72–77, https://doi.org/https://doi.org/10.1016/j.gexplo.2016.08.014, 2016.

Yoshimura, A., Suemasu, K., and Veiga, M. M.: Estimation of Mercury Losses and Gold Production by Artisanal and Small-Scale Gold Mining (ASGM), Journal of Sustainable Metallurgy, 7, 1045–1059, https://doi.org/10.1007/s40831-021-00394-8, 2021.

Yu, B., Li, G., Chen, S., and Lin, H.: The role of internal variability in climate change projections of North American surface air temperature and temperature extremes in CanESM2 large ensemble simulations, Climate Dynamics, 55, 869–885, https://doi.org/10.1007/s00382-020-05296-1, 2020.

Yue, F., Angot, H., Blomquist, B., et al.: The marginal ice zone as a dominant source region of atmospheric mercury during central Arctic summertime, Nature Communications, 14, 4887, https://doi.org/10.1038/s41467-023-40660-9, 2023.

Zhang, L., Wang, S., Wang, L., Wu, Y., Duan, L., Wu, Q., Wang, F., Yang, M., Yang, H., Hao, J., and Liu, X.: Updated Emission Inventories for Speciated Atmospheric Mercury from Anthropogenic Sources in China, Environ. Sci. Technol., 49, 3185–3194, https://doi.org/10.1021/es504840m, 2015.

Zhang, L., Zhou, P., Cao, S., and Zhao, Y.: Atmospheric mercury deposition over the land surfaces and the associated uncertainties in observations and simulations: a critical review, Atmospheric Chemistry and Physics, 19, 15 587–15 608, https://doi.org/10.5194/acp-19-15587-2019, 2019.

Zhang, P. and Zhang, Y.: Earth system modeling of mercury using CESM2 – Part 1: Atmospheric model CAM6-Chem/Hg v1.0, Geoscientific Model Development, 15, 3587–3601, https://doi.org/10.5194/gmd-15-3587-2022, 2022.

Zhang, Y., Jacob, D. J., Horowitz, H. M., Chen, L., Amos, H. M., Krabbenhoft, D. P., Slemr, F., St. Louis, V. L., and Sunderland, E. M.: Observed decrease in atmospheric mercury explained by global decline in anthropogenic emissions, Proceedings of the National Academy of Sciences, 113, 526–531, https://doi.org/10.1073/pnas.1516312113, 2016.

Zhang, Y., Zhang, L., Cao, S., Liu, X., Jin, J., and Zhao, Y.: Improved Anthropogenic Mercury Emission Inventories for China from 1980 to 2020: Toward More Accurate Effectiveness Evaluation for the Minamata Convention, Environmental Science & Technology, 57, 8660–8670, https://doi.org/10.1021/acs.est.3c01065, pMID: 37262354, 2023.

Zhao, Y., Wang, S., Duan, L., Lei, Y., Cao, P., and Hao, J.: Primary air pollutant emissions of coal-fired power plants in China: Current status and future prediction, Atmospheric Environment, 42, 8442–8452, https://doi.org/https://doi.org/10.1016/j.atmosenv.2008.08.021, 2008.

Zhao, Y., Zhong, H., Zhang, J., and Nielsen, C. P.: Evaluating the effects of China's pollution controls on inter-annual trends and uncertainties of atmospheric mercury emissions, Atmospheric Chemistry and Physics, 15, 4317–4337, https://doi.org/10.5194/acp-15-4317-2015, 2015.

Zyśk, J., Roustan, Y., and Wyrwa, A.: Modelling of the atmospheric dispersion of mercury emitted from the power sector in Poland, Atmospheric Environment, 112, 246–256, https://doi.org/https://doi.org/10.1016/j.atmosenv.2015.04.040, 2015.

Table 2. Simulations performed with the GEOS-Chem model (v 12.08.01).

Simulations					
Simulations groups	**Chemistry scheme**	**Emissions input**	**Simulation years**	**Inventory Years**	**Meteorological Data**
Group *Inventories*	Br	AMAP/GMA	2013-2015	2015	~~MERRA~~ MERRA-2
	Br	EDGAR	2013-2015	2012	~~MERRA~~ MERRA-2
	Br	STREETS	2013-2015	2013-2015	~~MERRA~~ MERRA-2
	Br	WHET	2013-2015	2010	~~MERRA~~ MERRA-2
Group *Chemistry*	Br	AMAP/GMA	2013-2015	2015	~~MERRA~~ MERRA-2
	OH/O_3	AMAP/GMA	2013-2015	2015	~~MERRA~~ MERRA-2
	Br	EDGAR	2013-2015	2012	~~MERRA~~ MERRA-2
	OH/O_3	EDGAR	2013-2015	2012	~~MERRA~~ MERRA-2
	Br	STREETS	2013-2015	2013-2015	~~MERRA~~ MERRA-2
	OH/O_3	STREETS	2013-2015	2013-2015	~~MERRA~~ MERRA-2
	Br	WHET	2013-2015	2010	~~MERRA~~ MERRA-2
	OH/O_3	WHET	2013-2015	2010	~~MERRA~~ MERRA-2
Group *Meteo*	Br	AMAP/GMA	2015	2015	~~MERRA~~ MERRA-2
	Br	AMAP/GMA	2015	2015	GEOS-FP